1-1-2019

The Relative Contribution of Fixation Features, Activity, and Tibiofemoral Conformity on Initial Stability of Cementless Tibial Trays

James Sullivan Deacy
University of Denver

The Relative Contribution of Fixation Features, Activity, and Tibiofemoral Conformity on Initial Stability of Cementless Tibial Trays

Abstract

Initial stability of cementless total knee replacements (TKR) is critical to implant success as excessive motion between the bone and implant prevents bony ingrowth that is critical to the long-term survivability of cementless implants. Prior studies have shown that excessive micromotion causes fibrous tissue growth instead of beneficial bony growth. There are many factors that influence initial stability including the design of the tibial tray and the tibiofemoral articulations. Understanding the impacts of these design features on micromotion between the bone and implants is crucial to improving the performance of cementless TKR. Prior studies only tested for the effect of micromotions induced in the shear direction-in plane with the surface of the implant. Much of the micromotion in tibial trays is normal to the tibial plateau but the importance of normal micromotion is unknown. In this study, a validated finite element model of an AMTI VIVO knee simulator was used to load various implant designs in 6 degrees of freedom during activities of daily living. Micromotions were estimated for two cementless TKR designs. To test the contributions of individual fixation features, additional simulations were run with certain fixation features (pegs and stem) removed and micromotions, as well as forces through the fixation features, were compared with the nominal components. The effects of tibiofemoral conformity were tested by creating custom insert models to vary the anterior and posterior conformity of the insert to the femoral component and comparing the micromotions to a medium conformity insert. Overall, tibiofemoral conformity greatly influences micromotion and the cause of that seems to be the increased femoral condyle translations increasing the moment arm around the tray. Removal of individual fixation features did not have the impact expected because friction on the plateau appeared to compensate for the missing features. Axial and shear forces through the pegs and stem are controlled by different factors. Axial forces are determined by tray design while shear forces vary with the conformity of the tibiofemoral geometry.

Document Type

Thesis

Degree Name

M.S.

Department

Mechanical Engineering

First Advisor

Chadd W. Clary, Ph.D.

Second Advisor

Paul Rullkoetter Ph.D.

Third Advisor

Mohammad Matin, Ph.D.

Keywords

Cementless, Finite element analysis, Total knee replacement

The Relative Contribution of Fixation Features, Activity, and Tibiofemoral Conformity on Initial Stability of Cementless Tibial Trays

_____

A Thesis

Presented to

the Faculty of the Daniel Felix Ritchie School of Engineering and Computer Science

University of Denver

_____

In Partial Fulfillment

of the Requirements for the Degree

Master of Science

_____

by

James Deacy

March 2019

Advisor: Chadd W. Clary

Author: James Deacy
Title: The Relative Contribution of Fixation Features, Activity, and Tibiofemoral Conformity on Initial Stability of Cementless Tibial Trays
Advisor: Chadd W. Clary
Degree Date: March 2019

ABSTRACT

Initial stability of cementless total knee replacements (TKR) is critical to implant success as excessive motion between the bone and implant prevents bony ingrowth that is critical to the long-term survivability of cementless implants. Prior studies have shown that excessive micromotion causes fibrous tissue growth instead of beneficial bony growth. There are many factors that influence initial stability including the design of the tibial tray and the tibiofemoral articulations. Understanding the impacts of these design features on micromotion between the bone and implants is crucial to improving the performance of cementless TKR. Prior studies only tested for the effect of micromotions induced in the shear direction-in plane with the surface of the implant. Much of the micromotion in tibial trays is normal to the tibial plateau but the importance of normal micromotion is unknown. In this study, a validated finite element model of an AMTI VIVO knee simulator was used to load various implant designs in 6 degrees of freedom during activities of daily living. Micromotions were estimated for two cementless TKR designs. To test the contributions of individual fixation features, additional simulations were run with certain fixation features (pegs and stem) removed and micromotions, as well as forces through the fixation features, were compared with the nominal components. The effects of tibiofemoral conformity were tested by creating custom insert models to vary the anterior and posterior conformity of the insert to the femoral

component and comparing the micromotions to a medium conformity insert. Overall, tibiofemoral conformity greatly influences micromotion and the cause of that seems to be the increased femoral condyle translations increasing the moment arm around the tray. Removal of individual fixation features did not have the impact expected because friction on the plateau appeared to compensate for the missing features. Axial and shear forces through the pegs and stem are controlled by different factors. Axial forces are determined by tray design while shear forces vary with the conformity of the tibiofemoral geometry.

ACKNOWLEDGMENTS

I would like to thank my advisor, Dr. Chadd Clary, for all his help as I restarted my thesis after a five-year hiatus. Also, Dr. Paul Rullkoetter for all his help when I first started my degree and for serving on my defense committee.

I also would like to thank Dr. Mohammad Matin for serving as my committee chair.

All the members of our research group have been very helpful and have made this an enjoyable place to work on my thesis.

Finally, I appreciate Depuy Synthes for supporting this project and so much of the work we do here.

TABLE OF CONTENTS

LIST OF FIGURES

CHAPTER 1. INTRODUCTION

1.1 Introduction

The use of total knee replacements (TKR) has increased greatly over the years due to an aging and active population and increases in obesity. TKR has been especially common in cases of severe knee arthritis. TKR is an expensive procedure but has been found to be very safe and its benefits to society outweighing the costs (Slover and Zuckerman 2012).

The knee joint contains three bones - the femur, tibia, and patella. TKR replaces the articular surfaces of the femur, tibia, and, optionally, the patella. The femoral component is typically metallic, while the tibial replacement typically has a metallic tray to connect with the tibial bone and a polyethylene insert to articulate with the femoral component. Among the challenges of TKR success is achieving strong fixation of the implants in the bone.

There currently are two main strategies used for fixation of TKR. The first employs polymethyl methacrylate bone cement to attach the implants to the bone and the other is biologic (cementless) fixation where the bone grows into the implant over time. Cemented TKR are the preferred choice of many surgeons because they are more stable immediately after implantation and the cement fills the gaps between the implant and bone left by imprecise cuts (Crook et al. 2017). However, concerns remain over their long-term survivability especially as younger and more active patients are having TKR.

Cemented implants can also be prone to aseptic loosening, which causes failure when the bone degrades around the cement.

Cementless implants have recently shown promise in overcoming these issues despite early failures (Dalury 2016). Years of success of cementless hip implants and recent improvements in porous materials and manufacturing techniques have renewed interest in cementless knee implants. In particular, cementless implants using these new technologies may increase bony ingrowth and thus, without the drawbacks of bone cement, improve survivability over cemented TKR (Findlay et al. 2004). Bony ingrowth is critical to the success of cementless TKR and only occurs with good initial fixation and immobilization of the implant relative to the bone during the first six weeks after surgery (Chong, Hansen, and Amis 2010). Micromotions between the bone and implant greater than 150 μm have been shown in canine studies to cause fibrous tissue growth in lieu of bony growth, creating a weaker connection between the bone and implant (Pilliar, Lee, and Maniatopoulos 1986; Jasty et al. 1997). These studies examined micromotion in the shear direction rather than the normal direction. Shear micromotion is movement of the implant relative to the bone in plane with the contacting surfaces, and normal micromotion is separation of the implant from the bone normal to the contacting surfaces. The distinction between the two types of micromotion is important for TKR because tibial trays experience normal micromotions on the plateau as well as shear micromotions. This is unlike hip replacements, which use a rod in a shaft, the conditions of these canine studies.

Fixation of the tibial tray to the tibia has been the primary area of concern with cementless TKR and has, therefore, been the focus of many studies. Cementless femoral components have had proven success and benefit from more inherent stability compared with tibial trays (Crook et al. 2017). The femoral implant covers the anterior, distal and posterior surfaces of the distal femur. This contact on opposing sides of the bone provides much of the stability to the femur. The tibial tray, however, lies on a single planar surface of the proximal tibia and experiences varying loads across the surface of the implant producing flexion-extension (FE) and varus-valgus (VV) moments. Tibial trays use cuts into the cancellous bone and features to improve attachment to the bone and resist these loads. Current cementless tibial tray designs employ various techniques to improve initial fixation with the bone including central stems, pegs, and keels with interference fits (Figure 1-1).

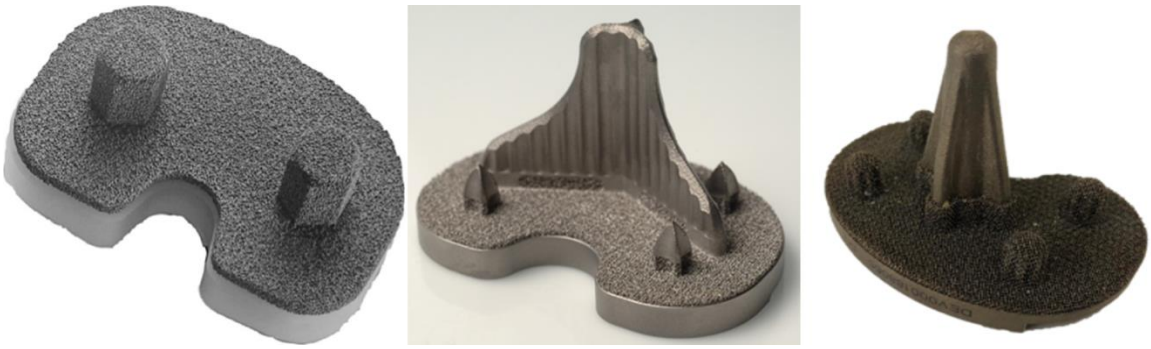

Figure 1-1: Current cementless tray designs: NexGen (Zimmer Biomet, Warsaw, IN) with two hexagonal pegs, Triathlon (Stryker, Kalamazoo, MI) with a central keel/stem and four cruciform pegs, and Attune (Depuy Synthes, Warsaw, IN) with a central stem and four cylindrical pegs.

Tibiofemoral articular geometries and the relative conformity between the femoral component and insert could have a large impact on the initial fixation of the tray, but these effects have not been adequately investigated. The geometries of the articular

surfaces affect the loads transmitted to the tray, but it is not clear if higher or lower conformity is better for initial fixation. For higher conformity geometries, it is possible that the anterior-posterior and medial-lateral forces will be greater and create moments that will rock the tray. On the other hand, higher conformity could constrain the femoral component enough to reduce the femoral condyle translation and reduce the moment arm of the compressive forces about the center of the tray. For lower conformity, the theories are the opposite. Anterior-posterior and medial-lateral forces will be lower, but the compressive forces will be acting further from the center of the insert.

Testing of initial fixation on cementless TKR has been performed both *in vivo* and *in vitro*. *In vivo* studies benefit from natural loading conditions and live bones, however, accurate assessment of loading and micromotion is difficult in living subjects and it is unethical to test unverified products on humans. *In vitro* studies have used synthetic foam bone structures as well as linear variable differential transducers (LVDT) or optical methods to measure micromotions around the rim of the tray, but many have simplified, axial-only loading conditions (Crook et al. 2017; Bhimji and Meneghini 2012). A more promising approach involves measuring micromotions during activities of daily living (ADL) such as gait, stair descent, and deep knee bend with *in vitro* studies and finite element models. The VIVO knee simulator (AMTI, Watertown, MA) can load knees in 6 degrees-of-freedom (DOF) with load or displacement control. It is also able to apply loads and displacements directly in anatomical coordinate systems. Synthetic bone substitutes have been used such as Sawbones™ (Pacific Research Laboratories Inc., Vashon Island, WA) to reduce the cost of testing the bone-implant interaction and

provide repeatability. Finite element models allow researchers to measure micromotion throughout the entire interface rather than only the outer rim of the tray and differentiate between shear and normal micromotions (Fitzpatrick, Hemelaar, and Taylor 2014). Examining micromotion across the entire interface provides important information about locations on the implants most susceptible to fibrous tissue growth associated with poor fixation. Finite element models have the additional benefit of being able to rapidly evaluate implant performance during the design phase in a cost-effective manner without exposing patients to experimental devices.

1.2 Objectives

The goal of this study was to understand the influence of TKR design on initial tibial tray fixation. This study used a previously validated finite element model of the 6 degree-of-freedom AMTI VIVO knee simulator during gait, stair descent, and deep knee bend with synthetic foam Sawbones™ and two brands of commercially available TKR, Attune (DePuy-Synthes, Warsaw, IN) and Triathlon (Stryker, Kalamazoo, MI) (Navacchia et al. 2018).

To accomplish this goal, this study accomplished the following objectives:

- Established baseline results for nominal Attune and Triathlon components during gait, stair descent and deep knee bend loading cycles using a validated finite element model;
- Evaluated fixation forces acting on each fixation feature to quantify their contributions to initial fixation;

- Examined whether poor bone quality around specific features impacts micromotion and the forces on the other features;
- Examined the influence of the tibiofemoral articulating surfaces on the micromotion of the tibial tray;
- Quantified the effect of conformity of insert to the femoral component on the magnitude of micromotions.

1.3 Thesis Overview

Chapter 2 presents a brief background of the use of cementless total knee replacements, prior *in vivo* and *in vitro* testing of cementless TKR, and a review of literature investigating micromotion in orthopedic implants.

Chapter 3 presents *The Relative Contribution of Fixation Features, Activity, and Tibiofemoral Conformity on Initial Stability of Cementless Tibial Trays,* which investigates how fixation features on the tibial tray and tibiofemoral geometry influence micromotion between the tray and tibia.

Chapter 4 Conclusions, including areas for future work.

CHAPTER 2. BACKGROUND INFORMATION AND LITERATURE REVIEW

2.1. Cementless Total Knee Replacement, *In Vivo*, *In Vitro* and Computational Testing

Cementless Total Knee Replacement

Cemented total knee replacements (TKR) have long been the preferred choice of surgeons over cementless implants due to their superior initial stability. However, concerns exist over the long-term durability of the cement, increased operating time while waiting for cement to cure, increased stress shielding, the required removal of more bone, and the risk of aseptic loosening. These concerns are becoming more acute as TKR are implanted in younger patients (who require more years of use) and heavier patients (who exert more stress on cement) (Dalury 2016). Recent improvements in porous materials and manufacturing technology have sparked renewed interest in cementless implants with the hope of improved bony ingrowth with the implant (Findlay et al. 2004). A randomized study of 100 TKR patients showed equivalent survivorship of cemented and cementless TKR after two years (Fricka, Sritulanondha, and McAsey 2015). Operating time can be decreased with cementless implants, but the accuracy of bone cuts is critical when cement is not able to fill in gaps between the bone and implant. Moreover, stability in the first six weeks after implantation is critical to long-term performance (Chong, Hansen, and Amis 2010).

In Vivo Testing:

Consistent with Wolff's Law, mechanical stimulation is a necessary stimulant for bone growth (Huiskes et al. 2000), but the threshold between helpful stimulation and excessive motion has been an area of interest. Studies in canines (Pilliar, Lee, and Maniatopoulos 1986; Jasty et al. 1997) have shown that micromotions greater than 150 microns inhibit the bony ingrowth which is critical for long-term implant stability. Jasty induced rotating oscillations to create micromotions of zero, twenty, forty or 150 μm on a cylindrical implant and found that as micromotions increased, bony ingrowth decreased. With higher micromotions, bony growth was replaced by fibrous tissues around the implant which compromised the connection. Pilliar found corroborating evidence in another canine study. They implanted porous devices loosely in the femurs of adult beagles and during the study, some of the implants grew cancellous bone growth around the implants while others had fibrous tissue attachment. After one year, they performed load-deflection tests with tension/compression loads of 20N. They found that samples with good bony ingrowth had maximum deflections of 28 μm, and samples with fibrous tissue attachment had 100-220 μm maximum deflections in compression and 50-310 μm maximum deflections in tension. Importantly, the fibrous samples showed little resistance to motion with forces up to 20N but were very stiff with greater forces and they concluded that further force would have produced very small additional deflections. Fibrous tissue growth in lieu of bone growth could impact the survivorship of the implant and lead to additional revisions. In all these studies, the induced micromotion was all in the shear direction-in plane with the face of the surface-and did not create normal

micromotion-a separation of the implant from the bone and the interface. This approach is representative of fixation forces for hip replacement stems as they have a cylindrical rod in a shaft like the devices used in these studies. For TKR, however, the tibial tray can experience moments that cause one edge of the tray to lift away from the bone. It is unknown if micromotions normal to the surface have the same impact on fixation as shear micromotions. A more recent *in vivo* study of 114 cementless Triathlon posterior stabilized (PS) implants (Harwin et al. 2013) found excellent fixation and survivorship on par or exceeding cemented implants.

In vivo testing has also been useful in quantifying joint loads during activities of daily living (ADL). One study used instrumented TKR in five subjects to quantify 6 DOF joint forces and moments during various activities including gait, stair descent and deep knee bend (Kutzner et al. 2010). Kutzner was the first to include forces and moments in all directions for multiple subjects as previous studies reported data for compression loads only. Kutzner's study was the basis for the Orthoload database which allows for public download of all the load data. These data have been used in several subsequent studies and are the basis for loading standards for testing implants.

Adoption of cementless TKA has possibly been hindered by early failures, but recent outcomes and the long-term success of cementless hip implants justify increased testing and use of cementless knee implants. *In vivo* studies are important in evaluating products in the market but are not useful in the design phase of new implant designs, which require alternative testing methods where patients are not exposed to unverified designs.

In Vitro testing:

In vitro testing involves experiments that do not involve live patients and has been used to evaluate micromotion for implants in the development. Experiments range from instrumented cadaveric specimens to tests with synthetic bones. Loading conditions can be simple static compressive loads to complex, dynamic loading conditions simulating ADL. The benefits of *in vitro* testing include lower costs, repeatability, and the ability to test development phase devices without ethical concerns.

One study compared cemented and cementless tibial trays in Sawbones™ (Crook et al. 2017). This study simulated eight weeks of *in vivo* function with 10,000 cycles of axial loads ramping between 20 and 2000 N at a rate of 1 Hz. The axial loads mimicked a gait cycle without other motion allowed at the femur. Superior-inferior motion was measured at five locations around the outer rim of the tray using linear variable differential transducers (LVDT) attached to measure linear motion of the tray relative to the base of the apparatus during first, 5,000th, and 10,000th cycles. This method measured how much the entire bone-implant construct compressed and was unable to differentiate relative motion at the interface between the bone and tray, which influences bone ingrowth. This study found all micromotions to be compressive. The largest micromotions were on the anterior face of the tray, which is also where differences between cemented and cementless micromotions were greatest. The greatest differences in micromotion between cemented and cementless components were less than 150 microns. They noted that this difference may be difficult to detect during implantation but could still interrupt fixation. Furthermore, spatial variation in micromotion magnitude

may result in varying levels of fixation across the tray. It is also possible that all the motion measured in this study was due to compression of the sawbones rather than micromotion at the interface.

Bhimji and Meneghini tested new implant designs with more complex and physiologically realistic loading conditions in sawbones (Bhimji and Meneghini 2012). They compared a tibial tray design that had a central keel with a design that had cylindrical pegs under each condyle to aid in deciding on a fixation strategy for their final design. The study started with axial loads on the lateral condyle cycling between 115 and 1150 N and then repeated on the medial condyle. They then added a posterior-stabilized (PS) femoral component and an insert, which was tested using a loading profile representing a stair descent activity. Their stair descent profile applied a compressive load, AP loads, and IE angular displacements. They fixed the flexion angle at 72 degrees where the post and cam were engaged, the condition with the greatest potential for rocking between the tray and bone. They found significantly higher micromotions with the stair descent loading compared with the axial loading, and higher micromotions for the two-peg tray compared with the keel tray during the stair descent. Interestingly, the micromotions during the axial loads on the medial and lateral condyles were similar between the two tray designs, highlighting that differences between devices may only appear with certain tests. This study was later replicated (Bhimji and Meneghini 2014) to compare Triathlon™ (Stryker, Kalamazoo, MI), with a keel and 4 pegs, and NexGen™ (Zimmer Biomet, Warsaw, IN), with two hexagonal pegs (Figure 2-1). Results indicated

that NexGen™ was more prone to the rocking motion that created anterior liftoff during the stair descent loading than Triathlon™.

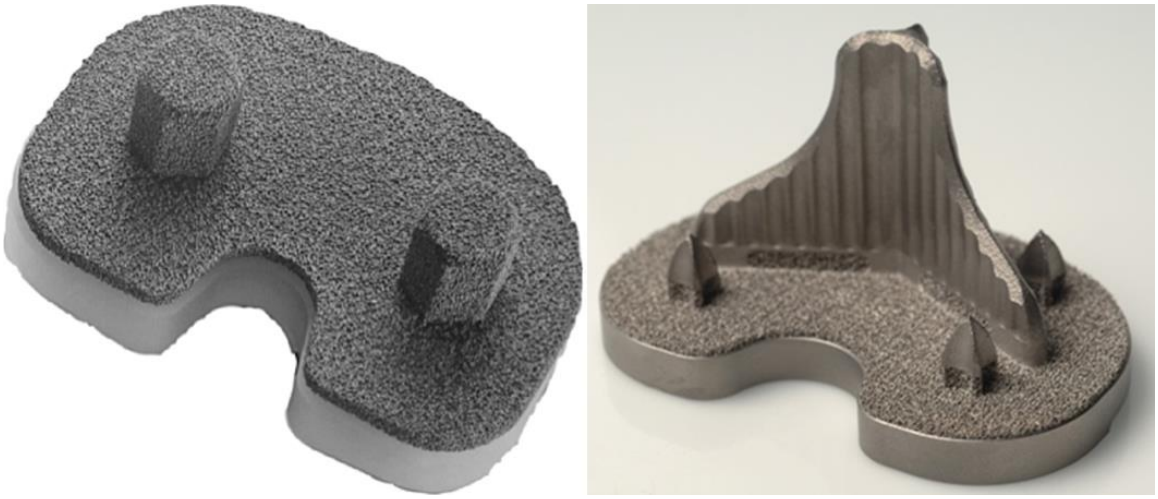

Figure 2-1: Fixation features on NexGen (left) and Triathlon cementless trays compared in Bhimiji and Meneghini's study

There have been several successful efforts to create *in vitro* testing systems with dynamic loading profiles that simulate ADL. Some systems simulate natural knee loads by applying loads at hip and ankle joints. An early example was the Oxford rig (Zavatsky 1997) which successfully simulated natural loads in the hip and ankle, and therefore, created accurate loads in cadaveric knee specimens. Subsequently, the Kansas Knee Simulator (Clary et al. 2013), among others, allowed for more complex multi-axis loads at the hip and ankle. In addition, they used the quadriceps tendon to physiologically load the knee. These testing systems improved the ability to predict kinematics and loads of developmental implant designs and were used with computational models to evaluate stresses in bones and implants. Additional efforts have been made to create loading profiles for activities such as turning and pivoting and those loading profiles were incorporated into ASTM standard F3141-15 (Proctor 2011). Another study used the

Orthoload database to develop loading profiles for axial forces, anterior-posterior forces, medial-lateral forces, and internal-external moments and kinematic profiles for flexion-extension for gait, stair descent, stair ascent, pivot turn, and crossover turn activities. Authors proposed adding the additional activities to gait because level gait accounts for only 54% of the activities of daily living (Van Valkenburg et al. 2016). AMTI created the VIVO, a 6 DOF knee simulator that can directly apply the loads and motions prescribed by the ASTM standards (VIVO, AMTI, Watertown, MA). The VIVO allows for joint loads and/or kinematics to be directly applied in the Grood and Suntay coordinate system (Grood and Suntay 1983) in any combination of the 6 DOF. The VIVO is entirely servo-controlled and contains a load sensor in the tibial fixture used to achieve the target joint loads (Figure 2-2).

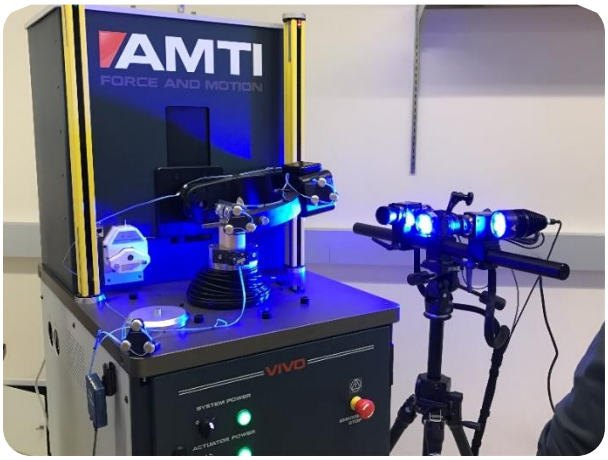

Figure 2-2 AMTI VIVO knee simulator with DIC motion capture system

A recent study used the VIVO simulator to evaluate current and developmental cementless tray designs from Stryker, DePuy, and Zimmer implanted in Sawbones™ and the ADL loading conditions described in ASTM standard F3141-15 (Wilson 2018). Since the ASTM standards do not include varus-valgus loading, this study used the averages

from the Orthoload patients to have loads or displacements in all 6 DOF. Digital image correlation (DIC) was used to measure displacement between the tray and the bone around the rim. Results of this study showed that increased micromotions were correlated with large femoral anterior-posterior translations while compressive load was high. These results indicate that tibiofemoral articulations have a large impact on micromotion at the tray.

Several methods have been used to measure micromotion at the bone-implant interface including linear variable differential transducers (LVDT) to measure the vertical displacement of the tray at five points around the rim (Bhimji and Meneghini 2012; Crook et al. 2017). This method fails to measure any differential motion at the bone-implant interface and seems to be mostly measuring the compressibility of the foam bone. Researchers have also used digital image correlation (DIC), a stereo-camera system capable of measuring 3D micromotion and strain at micrometer accuracy (Sutton et al. 2008). DIC, like the other methods discussed, can only measure micromotion on the visible areas of the system and thus cannot quantify micromotion over the entire interface.

Computational testing:

To address the shortcomings of physical testing, which measures micromotions only on the rim of the implants, researchers have used computational models. Computational testing allows for micromotion to be estimated across the entire interface of the implant and bone. One study validated a computational model of the VIVO knee simulator to be able to more efficiently evaluate long running experiments and to

complement the physical tests (Fitzpatrick et al. 2016). The study was able to achieve equivalent results as the physical tests and establish friction coefficients for the contact between implants. Another study used the VIVO simulator and this computational platform to create and validate a model to evaluate micromotion of cementless tibial trays (Navacchia et al. 2018). The study used the loading conditions developed by Van Valkenburg using the Orthoload database to run gait, stair descent, and deep knee bend loading cycles and evaluate micromotion along the anterior edge of the tray when implanted in a synthetic bone (Sawbones™, Pacific Research Labs, Vashon Island, WA). They used DIC to track the location of markers placed on the bone and tray near the interface and measure the separation between the bone and implant rather than the compression of the entire system as seen in other studies. Another study validated a computationally efficient finite element model to predict micromotions during gait (Fitzpatrick, Hemelaar, and Taylor 2014). They measured the micromotions at the bone-implant interface with relative displacements at node pairs across the interface. This model was able to accurately reproduce implant micromotions, indicating that this model is a good alternative to physical experiments during the developmental stages of implant design.

CHAPTER 3. THE RELATIVE CONTRIBUTION OF FIXATION FEATURES, ACTIVITY, AND TIBIOFEMORAL CONFORMITY ON INITIAL STABILITY OF CEMENTLESS TIBILA TRAYS

3.1. Introduction

The use of total knee replacements (TKR) has increased greatly over the years and has been used in patients with severe knee arthritis. Fixation of the implant to the bone is one of the key issues with TKR, especially on the tibial component. There are two main strategies for implant fixation, polymethyl methacrylate, an adhesive commonly called bone cement, and biologic or cementless fixation which achieve fixation over time as the bone re-grows into the implant. Cemented implants are the most common and are the choice of many surgeons due to their advantages in early stability and ability to compensate for surgical variability. However cemented implants can fail due to aseptic loosening and cement failure, especially in younger, more active patients (Crook et al. 2017). Recent development in cementless TKR technologies including porous materials and improved manufacturing techniques has increased the interest in cementless implants despite early failures (Dalury 2016).

The first six weeks after implantation are key for bony growth. Poor fixation during this period hinders bony growth (Chong, Hansen, and Amis 2010). Canine studies have shown that motions between the implant and bone greater than 150 μm create fibrous

tissue growth in lieu of bony growth, creating a weaker connection with the implant (Pilliar, Lee, and Maniatopoulos 1986; Jasty et al. 1997). These studies examined micromotion in the shear direction through rotation oscillation of the cylindrical implant rather than micromotions normal to the surface of the implant. Shear micromotion is movement of the implant relative to the bone in plane with the contacting surfaces, and normal micromotion is separation of the implant from the bone normal to the contacting surfaces. It is unknown if these normal micromotions have the same impact on bone growth as shear micromotions.

Various tibial tray designs have been created with the goal of promoting good initial fixation and robust bony growth around the implant. Several previous studies have examined their effectiveness (Crook et al. 2017; Bhimji and Meneghini 2012, 2014). They used synthetic foam bones designed to represent the proximal tibia with a cortical shell and a cancellous cortical foam core (Sawbones™, Pacific Research Laboratories Inc., Vashon Island, WA) to create a repeatable, cost-effective study. They found differing results for different loading conditions but were limited by applying simplified compressive-only loads rather than more realistic loading conditions mimicking activities of daily living (ADL), like gait (GT), stair descent (SD) and deep knee bend (DKB). *In vivo* anatomic joint loading was used to create the Orthoload database which provides loading data to the public for a variety of ADL (Kutzner et al. 2010). The Orthoload data was the basis for ASTM standard F3141-15 (Van Valkenburg et al. 2016) which is the loading standard for testing knee replacements. These loads can be input directly into the 6 degree of freedom (DOF) AMTI VIVO knee simulator (AMTI, Watertown, MA) in

anatomic coordinate systems. Finite element (FE) models have been used to examine additional micromotion characteristics not easily measured in physical experiments including micromotion across the entire bone-implant interface (Fitzpatrick, Hemelaar, and Taylor 2014). Micromotion across the entire interface provides important information about the areas on the implants most susceptible to the fibrous tissue growth associated with poor fixation.

Tibiofemoral (TF) articular geometries and the conformity of the insert to the femur (sagittal-plane femoral radius/insert radius) change the loads transmitted to the tray but their effects on tray fixation have not been investigated. One theory regarding conformity is that higher conforming inserts will increase the shear forces and that will thus increase micromotion. A competing theory is that less conforming inserts will allow for greater femoral translations and the change in the location of the contact forces will create a moment on the tray and cause rocking.

The objective of this study was to characterize the relative importance of the factors that contribute to good initial fixation of cementless tibial trays during ADL. The effects of bone quality, the accuracy of surgical fixation prep, the configuration of fixation features, and the conformity of the TF articular geometry were examined.

3.2. Methods

General Setup:

This study used a validated FE model of TKR components and synthetic proximal tibial bones (Figure 3-1) loaded with simulated cycles of ADL (Navacchia et al. 2018). The synthetic bones were proximal tibial Sawbones™ (Pacific Research Laboratories

Inc., Vashon Island, WA) constructs with a 12.5 pound per cubic foot (pcf) polyurethane cancellous foam core and a 50 pcf solid cortical shell sized to mimic a 9 mm deep resection plane of a medium sized tibia specimen. The Sawbones were 57 mm high and the proximal surface was 76mm by 46mm. This construct was chosen because it is commercially available and has been used in other studies for the same application (Bhimji and Meneghini 2012, 2014; Yildirim et al. 2016). Attune® (DePuy Synthes, Warsaw, IN) and Triathlon™ (Stryker, Kalamazoo, MI) fixed bearing, cruciate retaining TKR components with cementless tibial trays were the nominal components used for this study. The experiments were run using a 6 DOF AMTI VIVO™ knee simulator (AMTI, Watertown, MA) with five degrees of freedom using load control and the flexion-extension degree of freedom using displacement control. GT, SD, and DKB loading and kinematic profiles were derived from a combination of ASTM standard F3141-15 (Van Valkenburg et al. 2016), published telemetric implant data (Kutzner et al. 2010), and, since the ASTM standard does not have varus-valgus moments, those loads were taken as the average of the moments from the same Orthoload patients used by Van Valkenburg in developing the standard.

	Gait		Stair Descent		Deep Knee Bend	
Direction	Start of Cycle	Max. MM @ 16 % of Cycle	Start of Cycle	Max. MM @ 28 % of Cycle	Start of Cycle	Max. MM @ 50 % of Cycle
ML	-14 N	34 N	-9 N	41 N	-16 N	10 N
AP	-53 N	190 N	-43 N	203 N	10 N	13 N
SI	-863 N	-2195 N	-309 N	-3052 N	-1079 N	-2049 N
IE	1.9 N-m	-1.7 N-m	.5 N-m	1.4 N-m	.7 N-m	3.3 N-m
VV	.2 N-m	9 N-m	.9 N-m	.1 N-m	-2.9 N-m	11.0 N-m
FE	10 deg.	22 deg.	25 deg.	20 deg.	42 deg.	98 deg.

Table 3-1: Applied loading and displacement conditions at the start of each cycle and when micromotion was greatest.

The femoral implants and tibial inserts were meshed with 1-mm linear tetrahedral elements. The trays were meshed with 0.5-mm triangular elements to improve the accuracy of micromotion predictions along the interface with the bone. The bone constructs were meshed with linear, tetrahedral elements which coincided with the mesh of the tray at the mutual interface and had larger elements further from the tray for an average mesh size of 2-mm.

The TKR components had rigid body material definitions. The cortical and cancellous sections had linear elastic material definitions with elastic moduli of 1150 and 47.5 MPa and Poisson's ratios of 0.3 and 0.0, respectively. The bottom surface of the bone was encastred (fixed in 6 DOF). The cortical shell and cancellous core were meshed separately but were integrated via tie contact. The contact between the bone and tray was modeled with a friction coefficient of 1.0. The insert was beamed to the tray. Contact between the femoral component and insert had a friction coefficient of 0.01 because it best matched kinematic results from previous studies (Fitzpatrick et al. 2016).

Three cylindrical connector elements attached in series and configured along the Grood and Suntay axes (Grood and Suntay 1983) were used to apply loads and flexion-extension displacement to the femur. The first applied superior-inferior (SI) forces and interior-exterior (IE) moments. The second applied anterior-posterior (AP) forces and varus-valgus (VV) moments. The last connector applied medial-lateral (ML) forces and flexion-extension (FE) displacements.

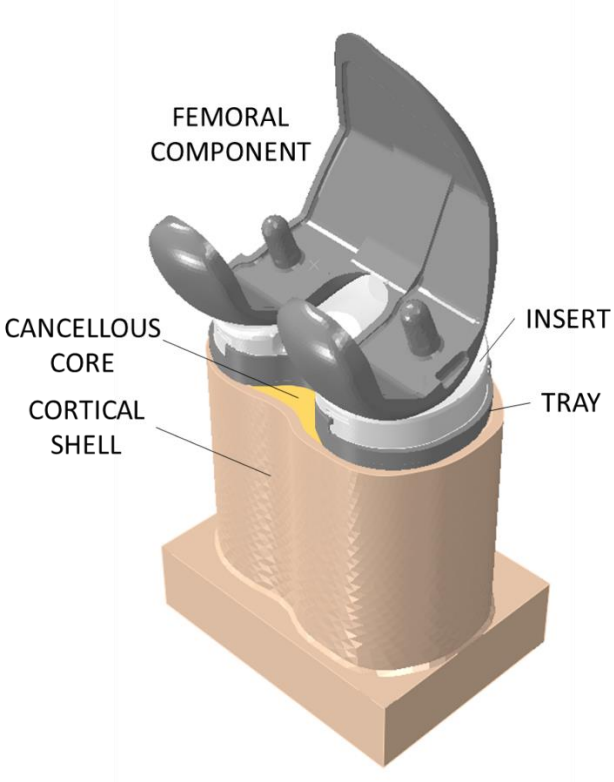

Figure 3-1: Sawbones™ construct with implanted tray, insert and femoral component.

Modeling of Fixation Features:

To measure the forces of individual fixation features, the fixation features were modeled with separate rigid body definitions for the proximal portion of the tray, the stem, and each of the four pegs (Figure 3-2). The pegs and stem were attached to the proximal tray using translator connector elements located at the center of each feature in plane with the distal face of the proximal tray which interfaces with the bone at the tibial plateau. The connector elements were locked in all six DOF and set up to report the forces and moments between the fixation features and tray. Forces were decomposed to axial and shear components with respect to the tray with normal components in the SI direction and shear in the transverse (ML/AP) plane.

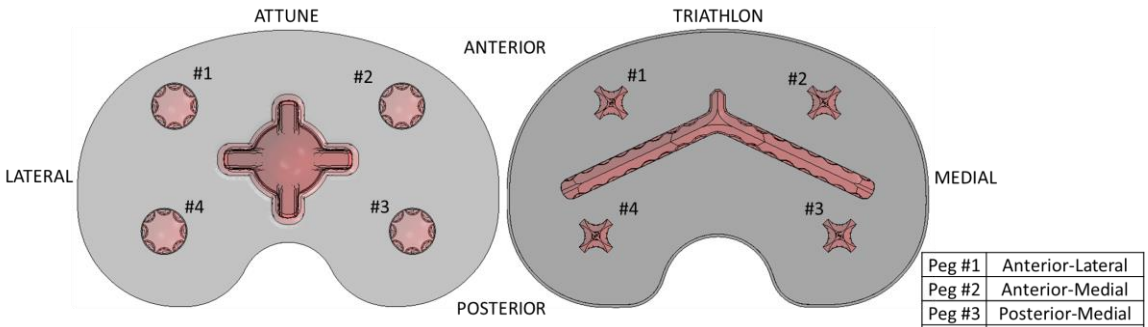

Figure 3-2: Top view of Attune and Triathlon cementless tray models

Metric Calculation:

Micromotion was calculated as the relative displacement between nodes on the tray surface at the interface with the bone and the nearest node on the bone surface. Micromotions were decomposed into normal and in-plane components relative to the surface normal at each node. For normal micromotions, separations of the surfaces were reported with positive values and compressive micromotions were reported with negative values and tracked separately. Micromotions were normalized from the start of each cycle to look at the relative movements occurring during the cycle. This means that all micromotions were zero at the start of each cycle and reported as relative displacements through the cycle. The loading conditions at the start of the cycle are seen in Table 3-1 along with the loading conditions when peak micromotions occurred. Micromotion was reported on the plateau only to provide for more consistent comparisons between models and to avoid ambiguous results around the sharp corners such as the scallops and points on the pegs.

The locations of the lowest points of the medial and lateral femoral condyles relative to the dwell of the tibial tray were calculated and the range of the locations was tracked in each simulation.

To provide consistent comparisons, all metrics were examined at the point in the loading cycles that saw the greatest micromotions (GT-16%, SD-28%, DKB-50%). Unless otherwise stated, all force and micromotion data presented were calculated at these points during the simulations.

Components Examined:

The Attune cementless tray (Figure 3-3, left) has a porous coating on the distal surface, four scalloped cylindrical pegs and a cruciform central stem with four tapered keels and porous coating for the proximal portion of the stem.

The Triathlon cementless tray (Figure 3-3, right) has a four smaller cruciform pegs and wide central keel. The central keel has two main sections extending posterior medially and posterior laterally from the center. The keel tapers towards the distal end of the tray.

Figure 3-3: Attune (left) and Triathlon tibial trays

The Attune femoral component has a distal sagittal radius of ~31 mm and a coronal radius of ~24 mm as measured from the arc radius at the most distal point of the condyle mesh in Hypermesh. The Attune insert has a distal sagittal radius of ~35 mm producing a conformity ratio of 0.88 and a distal coronal radius of ~25.5 mm and a conformity ratio of 0.94. Triathlon's femoral component has a distal sagittal radius of ~39 mm and a coronal radius of ~26 mm. The Triathlon insert has a distal sagittal radius of ~119 mm and a distal coronal radius of ~46 mm producing conformity ratios of 0.33 and 0.57, respectively. The minimum thickness is ~5 mm for the Attune insert and ~6 mm for the Triathlon inert.

Baseline Values:

The procedures described were performed with many different input parameters, such as adjusting the TF articulations and removing various fixation features. To establish baselines micromotion characteristics for each implant system, the GT, SD and DKB simulations were performed with the two nominal combinations of trays and TF

articulations: 1) Attune femoral component/insert and cementless tray; and 2) Triathlon femoral component/insert and cementless tray.

Swapping Tibiofemoral Geometries:

To investigate whether the femur and tibial insert or the tibial tray were driving the differences seen between Attune and Triathlon, additional tests were performed with Triathlon TF articulating surfaces on the Attune tray and the Attune TF articulating surfaces on the Triathlon tray. The results were normalized to the results from the nominal components.

Removal of Fixation Features:

To examine the impact of implanting a device in patients with regionally sub-optimal bone, simulations were run with each fixation feature independently removed from the model. For each implant set, individual fixation features were removed from the simulations to determine what removing those features would do to the forces in the other features. Simulations were run after removing one of the pegs and retaining the other three and the stem, removing the stem and retaining all four pegs, and removing all four pegs and retaining the stem (Table 3-2). All results were normalized to the nominal models.

Model Name	Features Removed	Features Remaining
Nominal	None	Stem, Pegs #1-4
No Peg #1	Peg #1	Stem, Pegs #2-4
No Peg #2	Peg #2	Stem, Pegs #1, 3, 4
No Peg #3	Peg #3	Stem, Pegs #1, 2, 4
No Peg #4	Peg #4	Stem, Pegs #1-3
No Stem	Stem	Pegs #1-4
No Pegs	All Pegs	Stem

Table 3-2: Configurations of fixation features removed for simulations

Tibiofemoral Conformity:

The effects of TF conformity on tray forces and micromotion were studied with nine different suppositional insert geometries with varying anterior and posterior sagittal radii (Figure 3-4). These insert geometries were tested with the Attune and Triathlon tibial trays but only the Triathlon femoral component to provide consistency of loading conditions and conformity ratios. Three different sagittal radii of curvature were used for both anterior and posterior aspects of the articulating surface (Figure 3-5; low conformity: 100 mm, ratio of 0.39; medium conformity: 70 mm, ratio of 0.56; high conformity: 40mm, ratio of 0.98) with a tangent point at the insert dwell. All inserts had the same coronal radius of 36 mm and coronal conformity ratio of 0.72. The inserts were chamfered on the anterior and posterior aspects to avoid sharp edges that could contact the femoral components and cause adverse contact conditions. The inserts were modeled with 8-noded hexahedral elements and used the same rigid body definitions and contact definitions as the nominal inserts. The inserts were placed to make the insert dwell points consistent with the nominal Attune and Triathlon inserts used in the previous simulations. All results were normalized to the results from the insert with medium anterior and posterior conformity, insert 2.

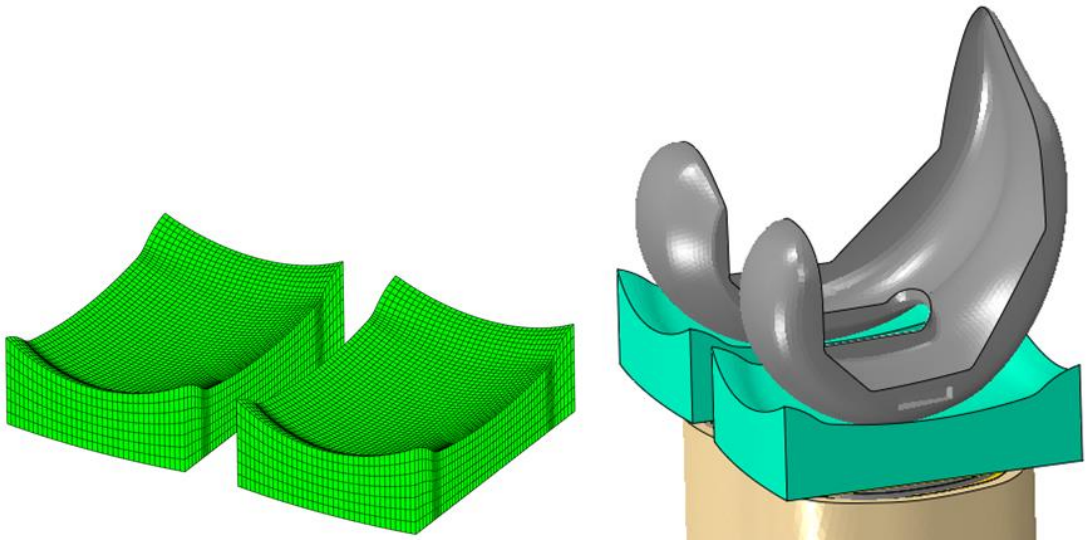

Figure 3-4: Mesh of low conformity insert (left), and in the model with the Sawbone, tray and femoral component.

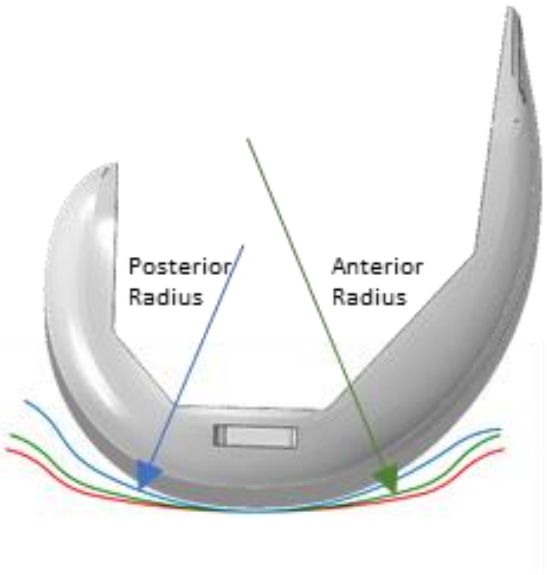

INSERT #	Anterior Conformity	Posterior Conformity
1	Low	Low
2	Medium	Medium
3	High	High
4	Medium	Low
5	Low	Medium
6	High	Low
7	Low	High
8	Medium	High
9	High	Medium

Figure 3-5: Comparison of insert sagittal conformity-red=low conformity, green=medium conformity, blue=high conformity.

3.3. Results

Nominal Attune and Triathlon Testing:

Normal micromotion increases linearly from the posterior to the anterior portion of the tray with peak normal micromotion occurring at the anterior edge of the tray and compression along the posterior edge for GT and SD. For DKB, the anterior lateral edge sees the highest normal micromotion and the posterior medial portion sees the most compression. Shear micromotion is more evenly distributed across the plateau of the tray and peaks occur on the lateral plateau for GT, the medial plateau for SD, and anterior rim for DKB (Figure 3-6).

The range of femoral condyle translations was greater with Triathlon than Attune and the lateral condyle was more posterior than the medial condyle for both components. SD had the greatest translations and DKB had the lowest (Figure 3-7).

Triathlon has generally higher forces through the stem than the Attune implants, especially shear forces (Figure 3-8). During GT and SD activities, shear forces through the stem follow similar profiles until about 60 N when Attune plateaus but Triathlon's shear force continues to increase. They also follow similar profiles at the end of each cycle once the Triathlon stem's shear force goes below the 60 N threshold. Triathlon has smaller pegs and a larger stem than the Attune implant, so the Triathlon stem takes a larger portion of the forces.

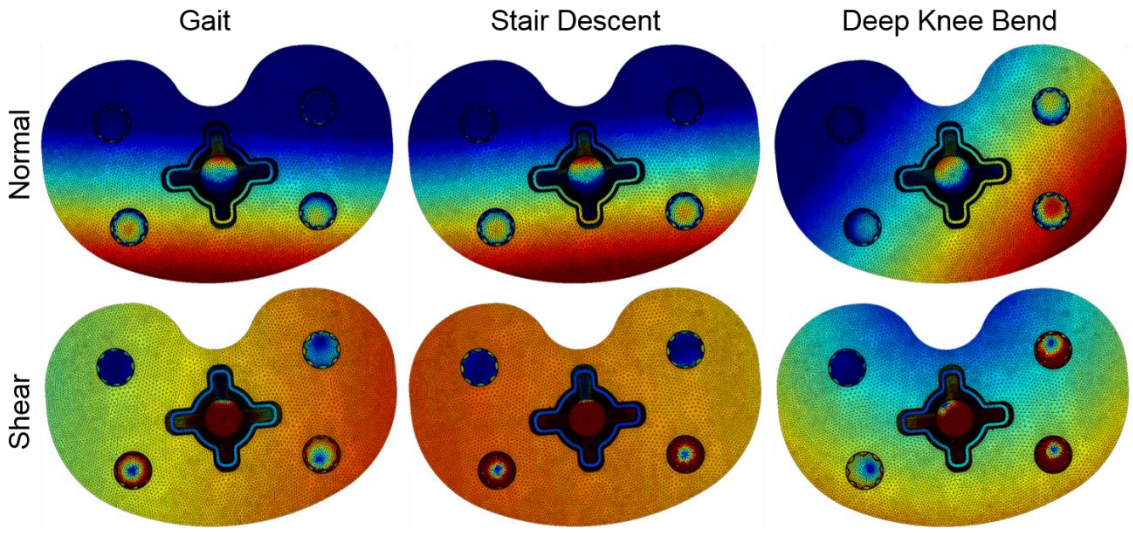

Figure 3-6: Micromotion tray plots showing areas of greatest (red) and lowest (blue) micromotion at 16%, 28% and 50% of cycle for GT, SD and DKB, respectively.

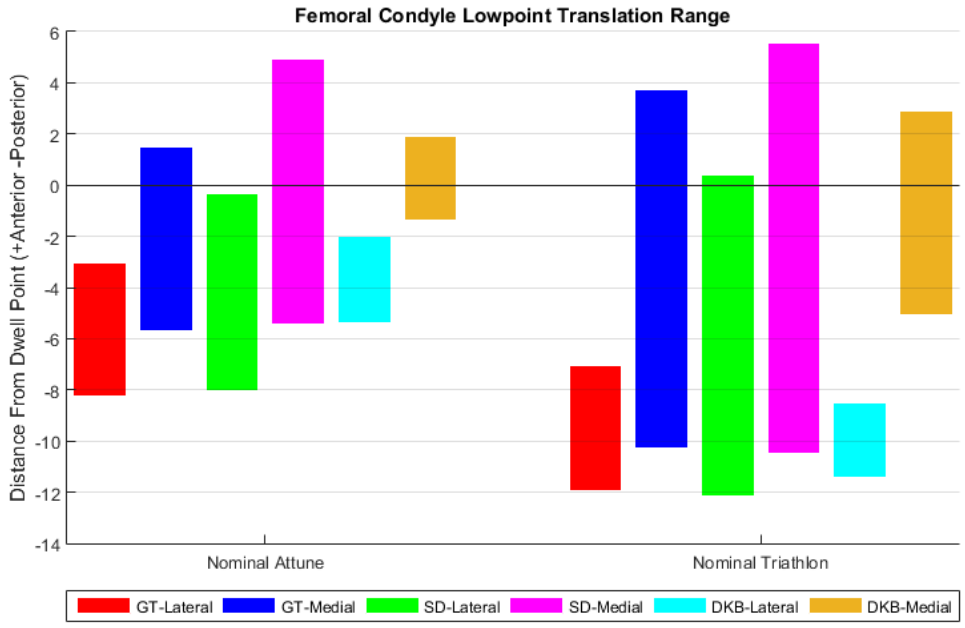

Figure 3-7: Range (mm) of Femoral Condyle Translation-Medial and Lateral Condyles.

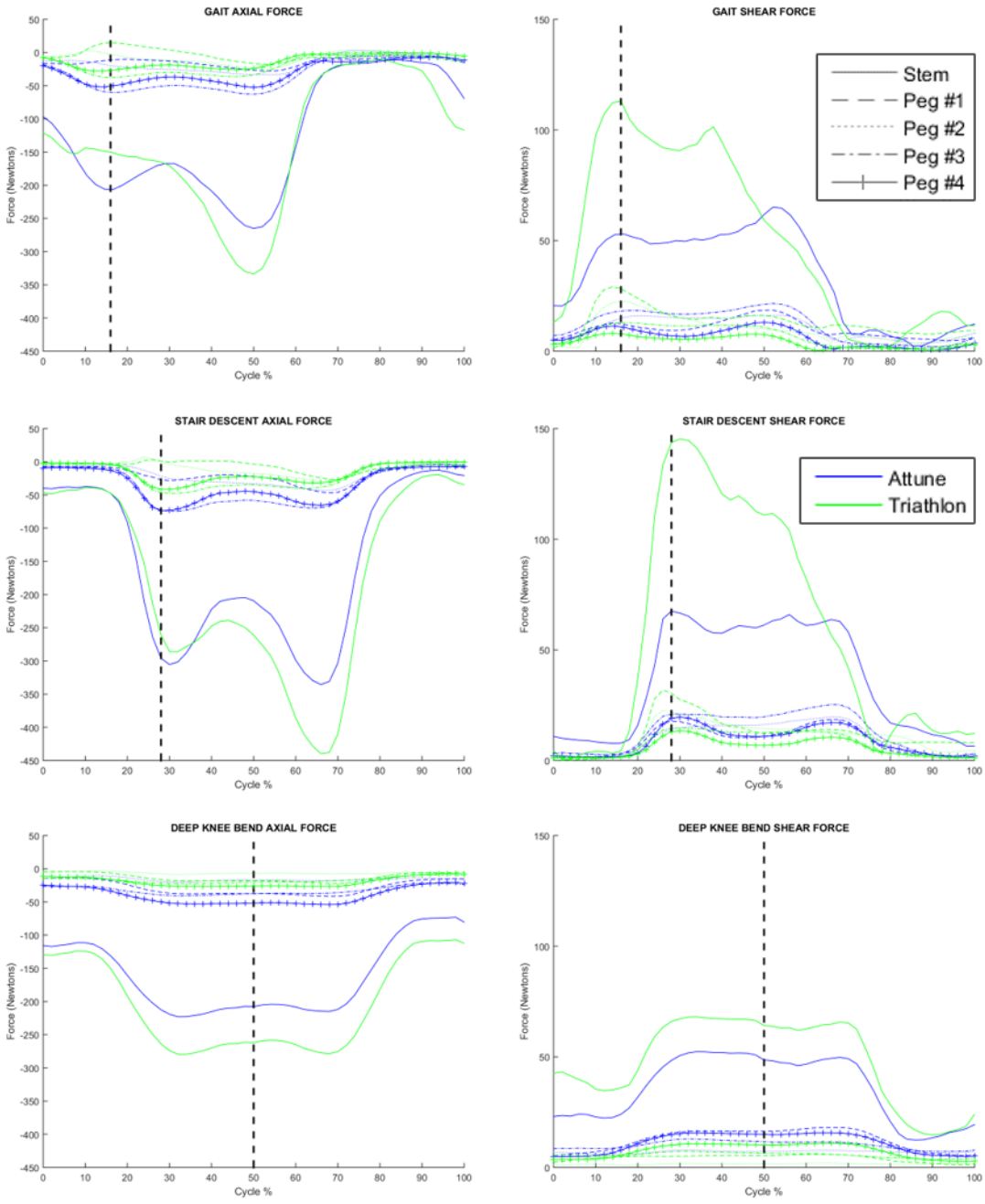

Figure 3-8: Peg and Stem Forces-Attune and Triathlon. Dashed vertical lines indicate location in cycle where peaks occur, and metrics are examined (16%, 28% and 50%). Negative axial forces are compression and positive are tension.

Swapping Tibiofemoral Geometries:

Pairing the Triathlon femoral component and tibial insert on the Attune tray produced higher normal micromotions for GT and SD and higher shear micromotions for all three activities than the nominal Attune components. (Normal—GT: 34%; SD: 30%; DKB: -11%. Shear—GT: 22%; SD: 32%; DKB: 2%). Conversely, pairing the Attune insert and femoral components with the Triathlon tray had the opposite effect on micromotion compared with the nominal Triathlon components. (Normal—GT: -41%; SD: -30%; DKB: 4%. Shear GT: -42%; SD: -61%; DKB: -6%). (Figure 3-9).

Axial forces through the stem decreased (50 N lower) with the Triathlon TF articulations on the Attune tray for GT and SD while shear force through the stem increased (60 N higher) and the DKB simulation had little change in force (less than 20 N). With the Attune TF articulations on the Triathlon tray, the stem had large increases in axial force for GT and SD (90 and 110 N, respectively), and decreases in shear force (60 and 80 N, respectively). For DKB, changes in axial and shear force through the stem were small. (Figures 3A-1-3)

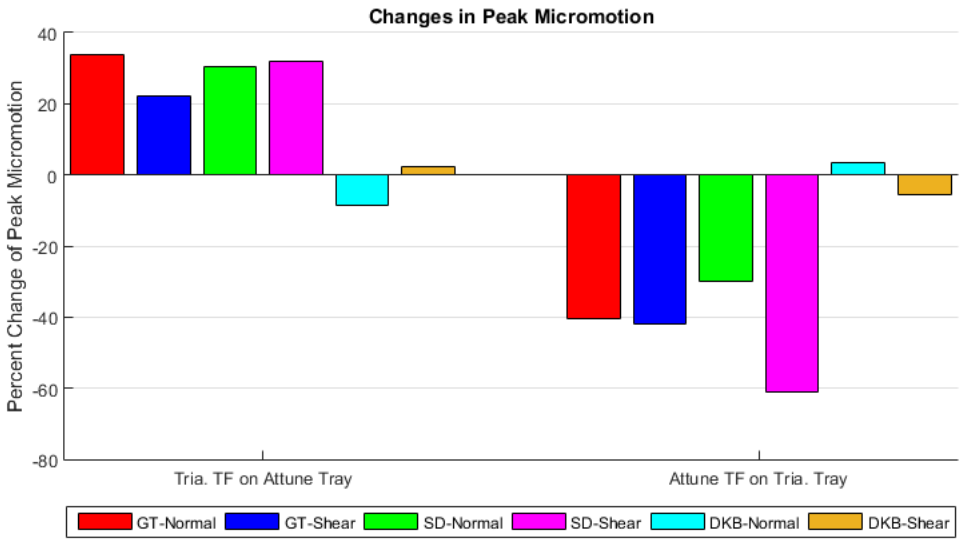

Figure 3-9: Change in micromotion-nominal components and swapped components at 16%, 28% and 50% of cycle for GT, SD and DKB, respectively

Removal of Fixation Features:

Removing fixation features on the Attune model did not have a large impact (<5% change from nominal components) on normal or shear micromotions apart from decreases when removing the posterior-lateral peg 4 (Normal—GT: -13%; SD: -18%; DKB: -23%. Shear—DKB: -15%) and increases when removing the stem during DKB (Normal: 13%; shear: 9%). The same decreases occurred when all four pegs were removed as when only peg 4 was removed (Figure 3-10).

During GT, Triathlon saw small changes in micromotions on the plateau from the nominal component when removing the pegs 2, 3 and 4 (less than 5%) but more substantial increases with anterior-lateral peg 1 removed, with the stem removed, and with all four pegs removed (Normal: 24%; 34%; 28%. Shear: 32%; 4%; 28%, for peg 1, stem, and all four pegs removed, respectively). SD had similar results with increases with

peg 1 removed, for the stem removed and for all four pegs removed (Normal: 8%; 17%; and 12%. Shear: 48%; 13%; 56%, respectively). The DKB cycle saw nearly identical normal micromotions for all simulations except when the stem was removed (7% higher). Shear micromotion during DKB all had similar results to the nominal components (less than 5%) (Figure 3-11).

Changes in the forces through the fixation features were small for all simulations with fixation features removed (less than ~15 N). The largest changes occurred when the stem was removed (max peg force changes ~5-10 N), and with all pegs removed (~10-15 N). (Figures 3A.4-9)

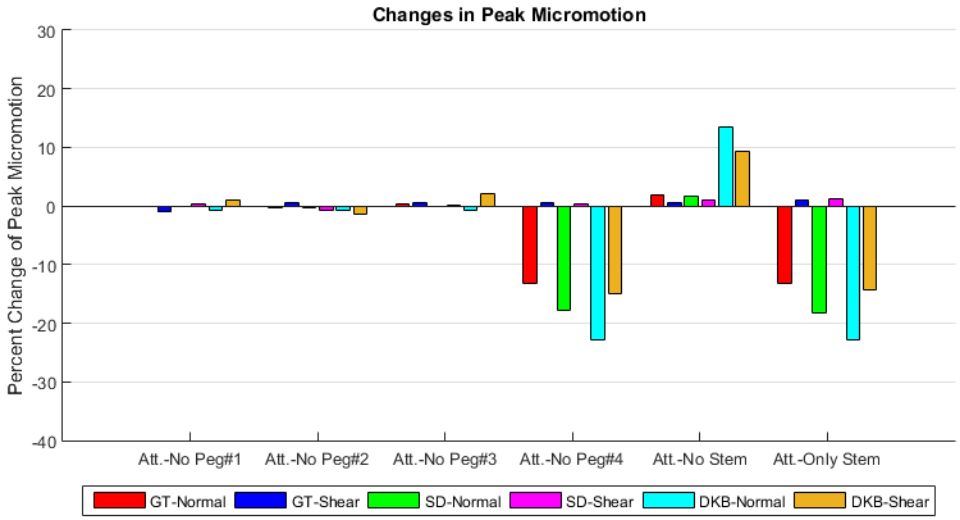

Figure 3-10: Change in micromotions from nominal components for Attune tray when features are removed at 16%, 28% and 50% of cycle for GT, SD, and DKB, respectively.

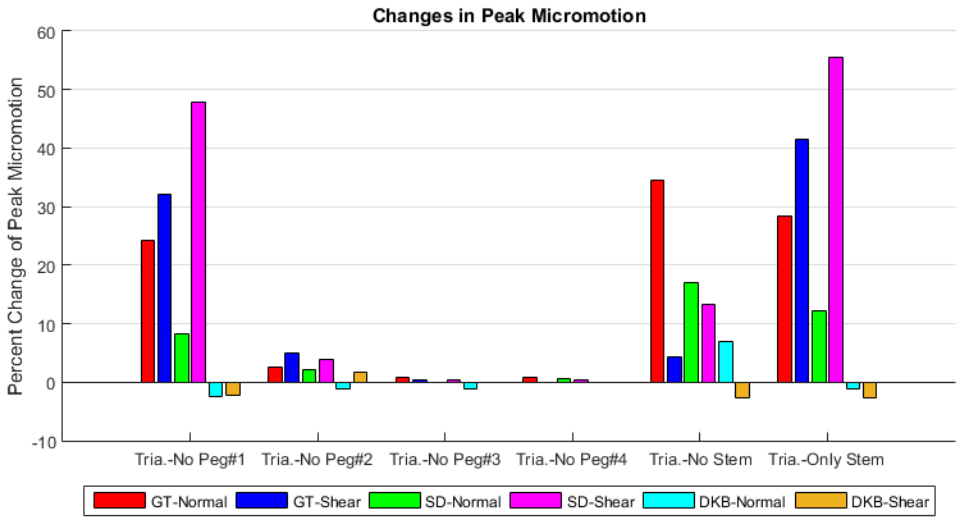

Figure 3-11: Change in micromotions from nominal components for Triathlon tray when features are removed at 16%, 28% and 50% of cycle for GT, SD, and DKB, respectively.

Tibiofemoral Conformity:

Changing the conformity of the TF articulation greatly affects the lowpoint translation of the femoral condyles (Figure 3-12). Inserts with low posterior conformity had the greatest posterior translation of the femoral condyles while inserts with low anterior conformities had the greatest anterior translation of the femoral condyles. High conformity inserts had the lowest femoral condyle translations.

For the simulations with the Attune tray, normal micromotion correlated with reduced posterior TF conformity strongly for GT and SD (R^2=0.872-GT; 0.933-SD; 0.425-DKB). Correlation coefficients were also high for shear micromotion during GT and SD (R^2=0.886-GT; 0.922-SD; 0.140-DKB) (Figure 3-15). Micromotion was not correlated with anterior TF conformity for normal (R^2=0.007-GT; 0.002-SD; 0.106-DKB) or shear micromotion (R^2=0.010-GT; 0.003-SD; 0.341-DKB) (Figure 3-16).

Similar results occurred with the Triathlon tray. Normal micromotion correlated with reduced posterior conformity for GT and SD but not DKB (R^2=0.933-GT; 0.944-SD; 0.182-DKB). Shear micromotion during GT and SD also had high correlation coefficients (R^2=0.934-GT; 0.940-SD; 0.444-DKB) (Figure 3-17). Micromotion was not correlated with anterior TF conformity for normal (R^2=0.005-GT; 0.001-SD; 0.090-DKB) or shear micromotion (R^2=0.001-GT; 0.000-SD; 0.342-DKB) (Figure 3-18). Micromotions increased as posterior radius increased for GT and SD.

With the Attune tray, low posterior conformity inserts had decreased axial forces through the stem (40 N lower), and the anterior pegs (10-15 N lower), and small increases in axial forces for the two posterior pegs for GT and SD. Those simulations had increased shear forces through the stem (50-60 N higher) and through the pegs (0-20 N higher). The high conformity inserts had small changes (less than 10 N) in axial forces through the pegs and stem and decreases in shear force through the stem during GT and SD (25-50 N lower). All DKB cycles had changes in force of less than 20 N. (Figures 3A.10-12)

Force changes followed a similar pattern for the Triathlon tray. During GT and SD, all inserts with low posterior conformity (inserts 1, 4 and 6) had decreases in axial and shear force through the stem (25-35 N lower) and had axial and shear force increases in the two posterior pegs (pegs 3 and 4) (35-45 N higher). The anterior pegs had smaller force increases of less than 10 N. Inserts with high posterior conformity (inserts 3, 7 and 8), saw opposite changes: small increases in stem forces, decreases (25-30 N lower) in the posterior pegs and smaller increases (~10 N) in the anterior pegs. The inserts with

medium posterior conformity had small changes in all forces except forces through the stem during SD with insert 9 (high anterior conformity and medium posterior conformity), which had decreases in axial force (~15 N lower) and shear force (~20 N lower). DKB did not produce clear patterns based on posterior conformity. All force changes were less than 40 N and the largest changes were seen in insert 6 which had low posterior conformity and high anterior conformity. (Figures 3A.13-15)

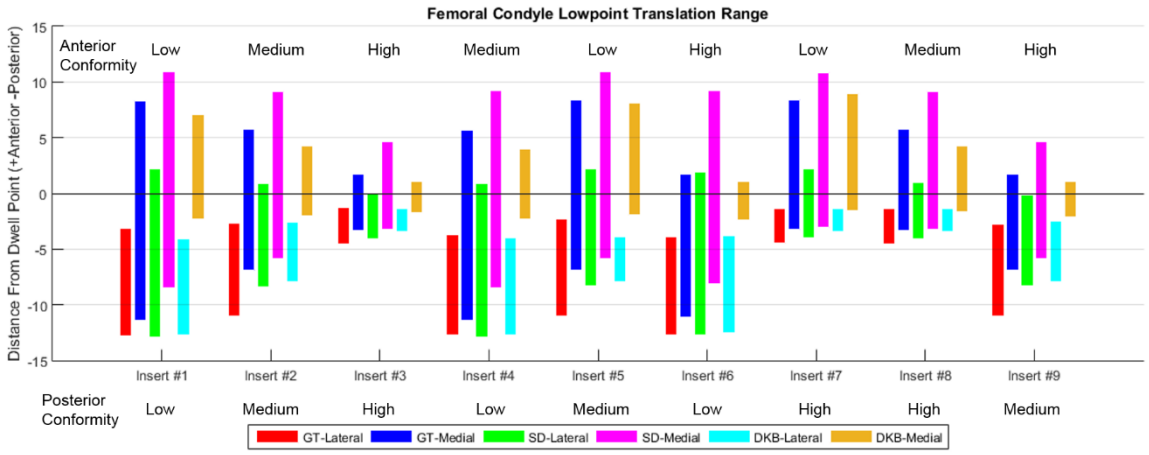

Figure 3-12: Femoral condyle lowpoint translation ranges (mm) from insert dwell points.

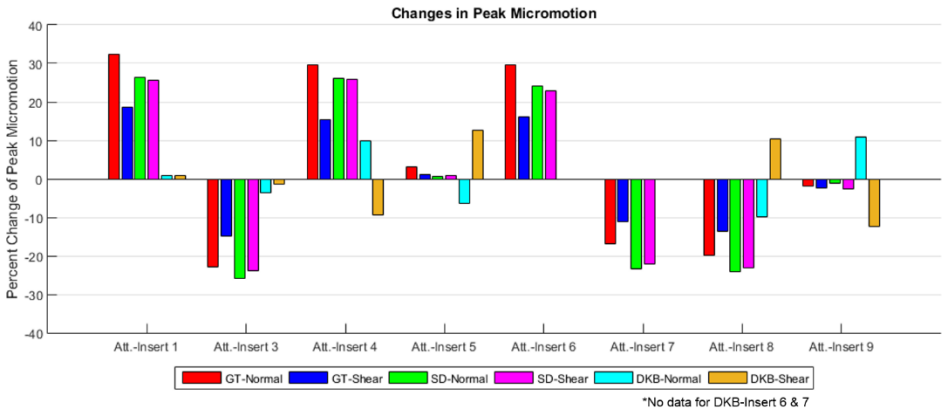

Figure 3-13: Change in micromotions from medium conformity insert (insert 2) for Attune tray with custom inserts at 16%, 28% and 50% of cycle for GT, SD, and DKB, respectively.

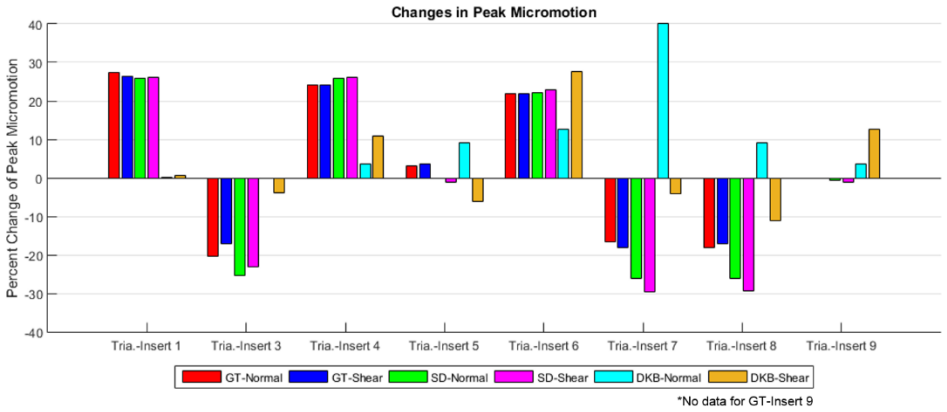

Figure 3-14: Change in micromotions from medium conformity insert (insert 2) for Triathlon tray with custom inserts at 16%, 28% and 50% of cycle for GT, SD, and DKB, respectively.

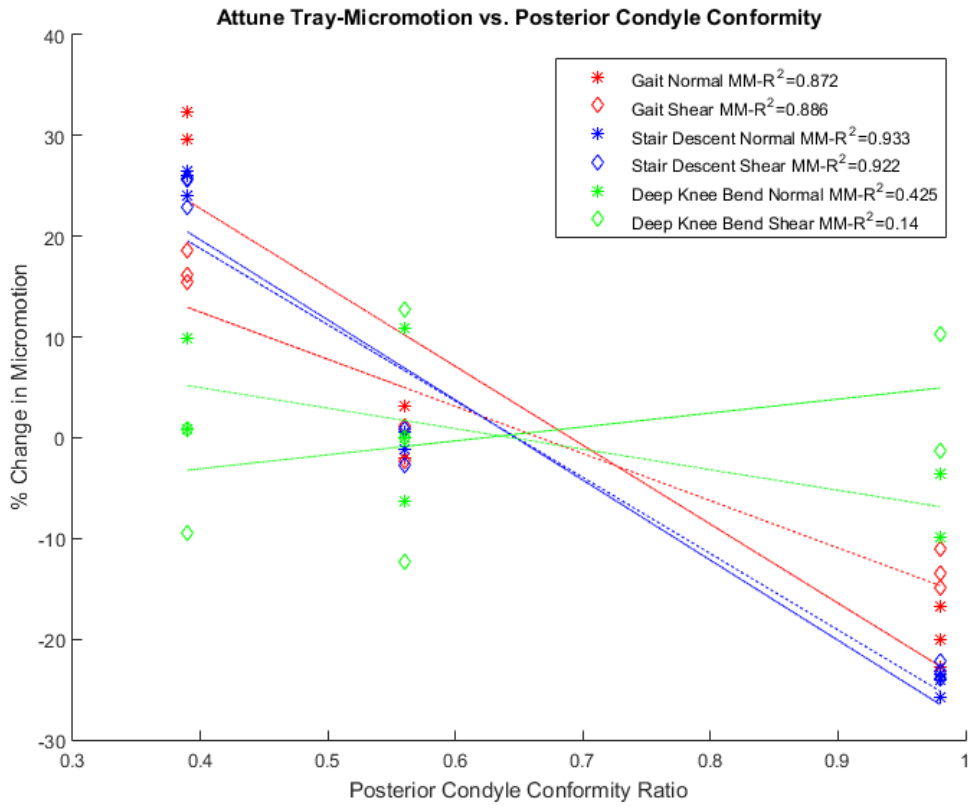

Figure 3-15: % change in micromotion (normalized to insert 2) vs posterior condyle conformity ratio for Attune tray.

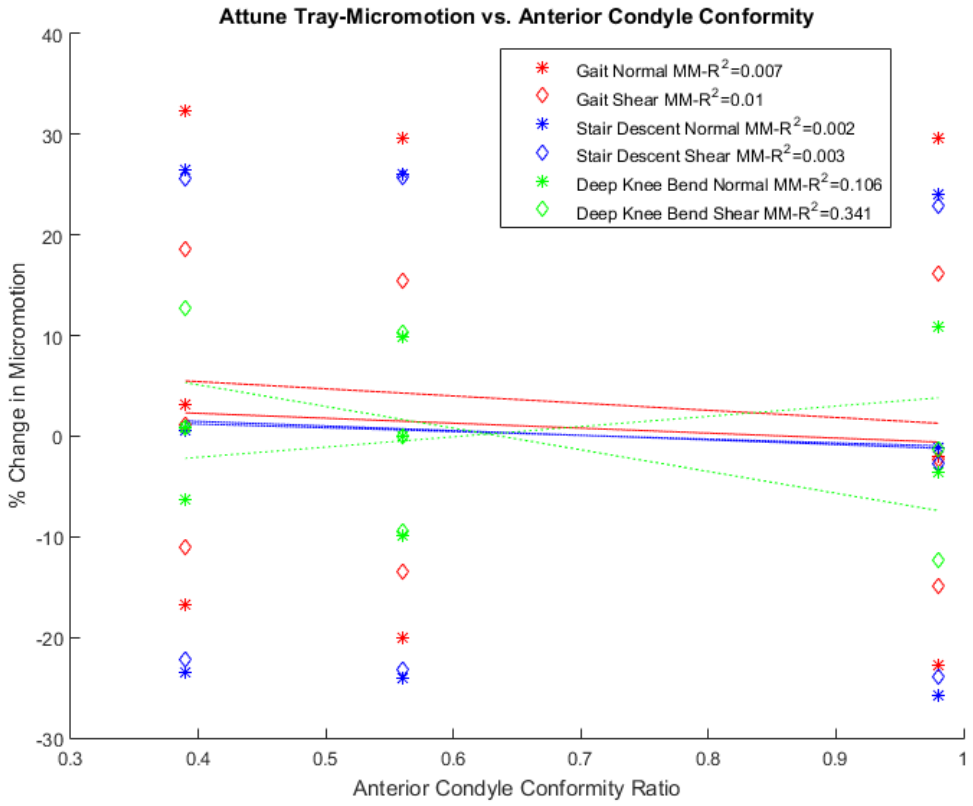

Figure 3-16: % change in micromotion (normalized to insert 2) vs anterior condyle conformity ratio for Attune tray.

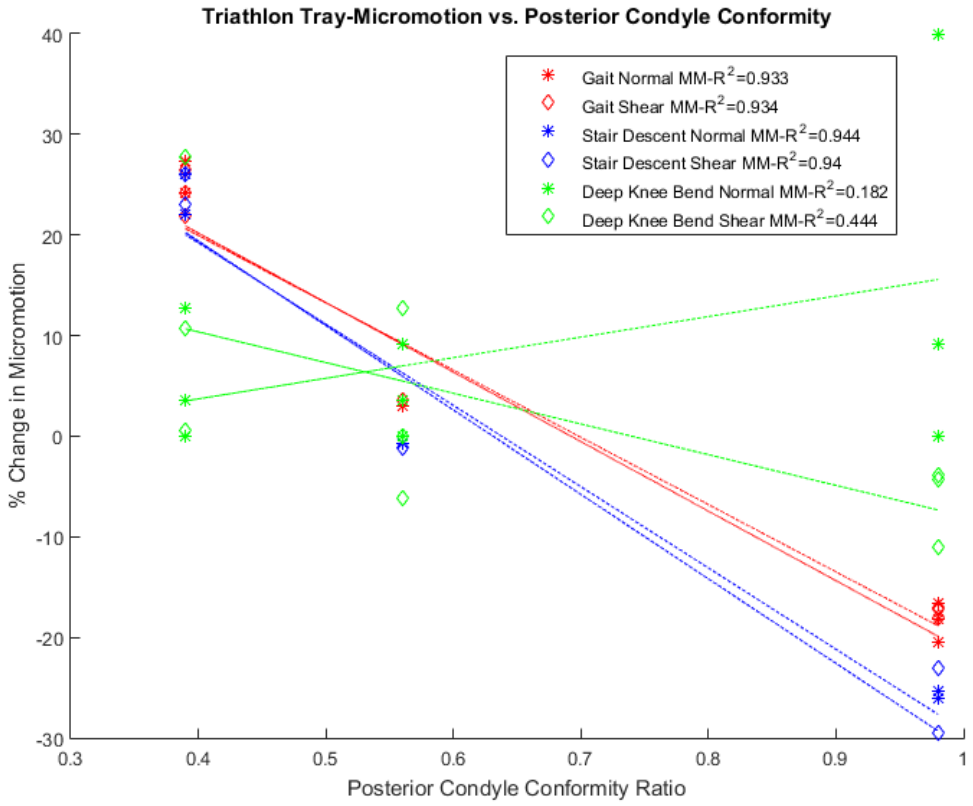

Figure 3-17: % change in micromotion (normalized to insert 2) vs posterior condyle conformity ratio for Triathlon tray.

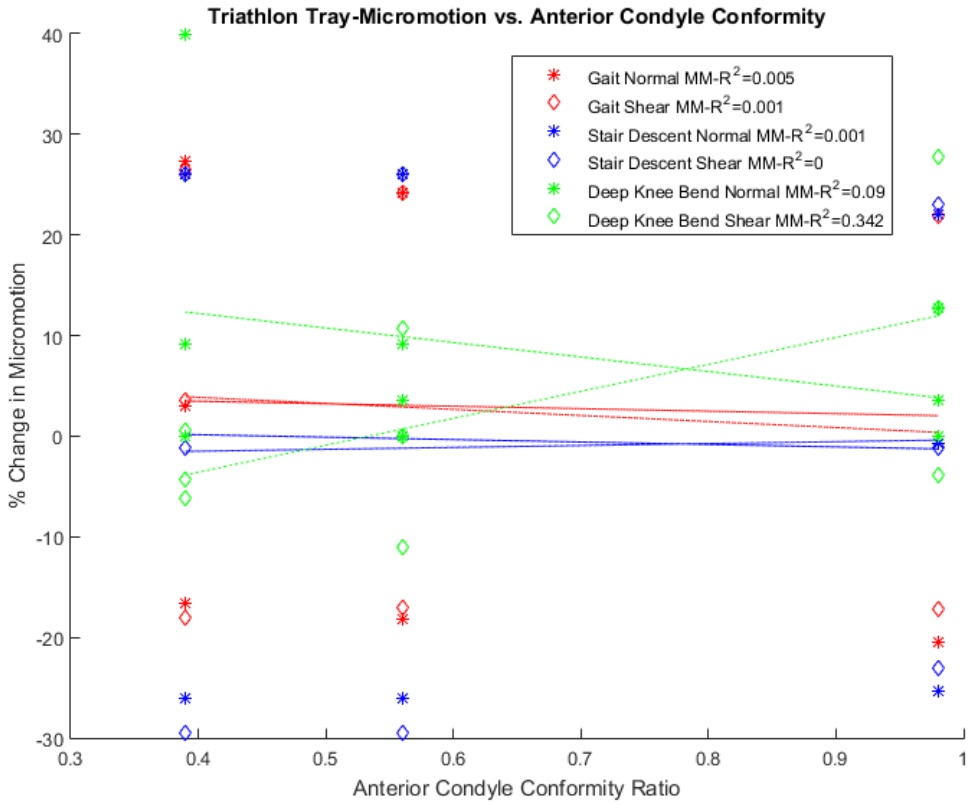

Figure 3-18: % change in micromotion (normalized to insert 2) vs anterior condyle conformity ratio for Triathlon tray.

Comparison of Conformity and Fixation Feature Effects:

The effects of TF conformity produced increases and decreases in normal and shear micromotion of ~25% for GT and SD with the Attune tray while removing the largest fixation feature, the stem, from the simulation produced increases of less than 5% (Figure 3-19). For DKB, removing the stem produced greater changes in micromotion compared with changing conformity (~10-15% and ~5%, respectively).

The Triathlon tray had increases and decreases of ~20% for GT and SD caused by changing conformity. Removing the stem produced the greatest increases in normal micromotions and removing the pegs produced the greatest increases in shear

micromotions (more than 40% for GT and SD). Micromotions did not have large changes during DKB for any of the simulations (Figure 3-20).

Similarly, changes in forces through the fixation features were much larger for the swapped TF models and TF conformity models (+/- 50-100 N) than when removing features (less than 10 N) (Figures 3A-16-21).

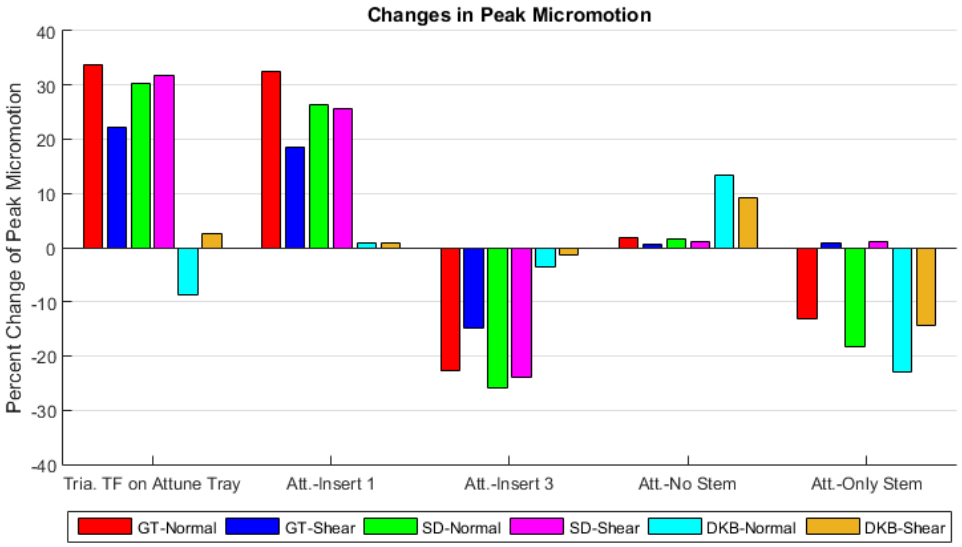

Figure 3-19: Comparison of changes in micromotion for conformity and removing of fixation features for Attune trays.

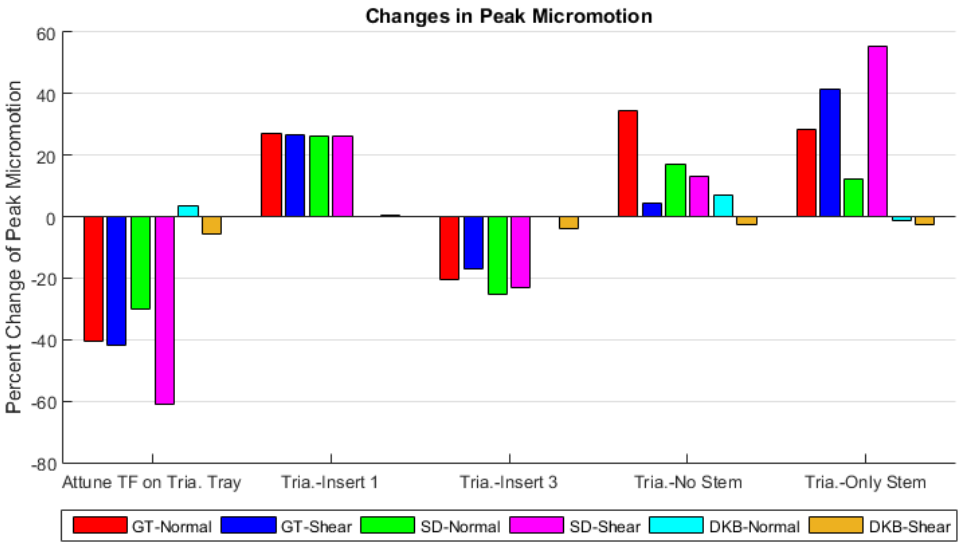

Figure 3-20: Comparison of changes in micromotion for conformity and removing of fixation features for Triathlon trays.

3.4. Discussion

This study suggests that micromotion is much more sensitive to changes in TF contact mechanics than to changes at the tray-bone interface. Loss of one of the pegs produced only incremental changes in micromotion across the plateau suggesting that frictional forces across the plateau are providing more stability during activity than the pegs. Likewise, forces in the remaining pegs and stem did not increase when other features were removed, and those forces were offset by increased frictional forces without an increase in micromotion. This means that patients with localized poor bone quality may not suffer more micromotions than patients with healthy bone. In contrast, changing the conformity of the TF articulation consistently caused increases and decreases in micromotion of 25-30%, much more than most of the results from removing

individual fixation features. These results are corroborated by the results when swapping TF components. The low conformity Triathlon TF greatly increased micromotion on the Attune tray while the higher conformity Attune TF decreased micromotion when paired with the Triathlon tray. Larger posterior femoral condyle translations allowed by lower conformity caused greater micromotions.

Tibia-Femur Swap:

The Triathlon femoral component and insert produced higher micromotions on both trays than the Attune components. The difference can be attributed to the less conforming geometry of Triathlon components compared with the Attune components. These results fit with the results seen when systematically varying TF conformity. When looking at peg and stem forces, the axial forces remain constant when changing the TF articulations while the shear forces appear much more dependent on the articulations than the tray. The geometries of both inserts are much more complex, with varying sagittal and coronal radii, than the inserts created in the conformity study, and, consequently, cannot be compared directly with the conformities of the simple inserts from the conformity study. The conformity ratios presented for the Attune and Triathlon inserts are only valid for small areas around the insert dwell points and quickly change as contact moves away from the dwells.

For all three activities, the axial forces through the stem and pegs are driven by the tray design while the shear forces are driven by the TF articular geometry. This could be due to the layout of features controlling the distribution of the axial forces while the TF conformity affecting the shear forces transmitted through the tray.

Conformity:

The conformity study clearly shows that inserts with more conforming posterior geometries produced lower femoral lowpoint translations and had lower micromotions with both tray designs. Prior to this study, one hypothesis was that more conforming inserts would produce greater moments on the tray and result in greater micromotions; however, the less conforming inserts allowed the low points of the femoral condyles to travel further posterior, increasing the moment arm of the compressive forces. Within the range of posterior condylar radii studied, micromotion decreased linearly as the posterior radius of the insert increased for GT and SD but not for the DKB loading cycle. For these tests, the anterior radius did not have an impact on micromotion most likely because during these tests there was no anterior TF reaction force, so the femur did not articulate with the anterior portion of the insert. Because of the clear correlation with posterior radius for two of the activities and the less sensitive results with DKB, several tests need to be performed to evaluate micromotion in a variety of loading conditions. It is also possible that loading conditions that produce contact with the anterior insert or greater posterior translation could produce different results and could be a better indication of performance for certain patients.

As with the results from the component swap study, conformity did not impact axial forces through the stem and pegs, but the lower conformity inserts had higher shear forces. These corroborating results support the hypothesis that more conformity will reduce shear forces but not impact axial forces. Since the forces applied to the joint are

the same for all the simulations, the location on the inserts of the contact force from the femoral components was a factor influencing shear forces the most.

Fixation Feature Removal:

When contemplating the effects of poor bone quality around individual fixation features, it was expected that incremental increases in micromotion and corresponding increases in the forces experienced by the remaining fixation features as others were removed would occur. What was found, especially with the Attune tray, was that removing certain features had little impact on micromotion. Forces through the remaining fixation features did not increase when the pegs were removed, and peg forces increased less than expected when the stem was removed from the simulations. This suggests that most of the force is being resisted by friction in the plateau. The reduction in micromotion with the posterior-lateral peg 4 removed from the simulation is difficult to explain. The results are consistent when only peg 4 is removed from the simulation and when all four pegs are removed. It could be caused by a rocking motion around the peg when it is present that does not occur when it is removed, and the tray is resting evenly on the plateau of the bone. The micromotion occurs at the anterior edge of the tray in both cases. The location of the contact between the insert and femoral component remains directly above or anterior of the peg but the slope of the insert means that there is a resulting moment around that location. This moment appears to be what is creating the rocking motion around the posterior-lateral peg which produces the higher micromotions. This was not seen in the Triathlon components possibly because the relative size of the peg compared with the stem where the large stem of triathlon has a larger impact on

stability. Another possibility is the resultant force of Triathlon is not producing a rocking around the pegs.

Limitations:

This study had many limitations including the inability to validate micromotion values away from the visible edges of the tray and bone and simplified material definitions used for the bone and tray. While the model was verified for micromotion around the rim of the tray, there is no experimental data to compare the micromotion around the entire interface of the implant. Linear elastic material definitions of the foam bone could be affecting the results, especially looking at micron-level differences. This study only used one average placement of the implants and did not examine the effects of surgical variation in implantation position.

One of the drawbacks of the methods used for this study is the treatment of the contact of the removed features. Contact was removed between the bone and the fixation features but the contact between the bone on the plateau immediately around the removed features and the flat portion of the tray remained. It is likely that if the bone were regionally degraded it would not have good contact on the plateau or provide frictional resistance. Additionally, contact pressures on the plateau around removed features were greater so it would be beneficial to repeat this study with reduced contact pressures immediately around the removed features. This modified study could better represent inaccurate surgical cuts that create gaps between the fixation features and the bone rather than poor bone quality.

The insert geometries used in this study were useful for examining the effects of TF sagittal conformity on micromotion of the trays, however, coronal conformity was not varied, and these inserts do not represent real insert geometries. Further efforts should be made to create parametric representations of real inserts that could vary the more complicated features found in modern insert designs. Anterior conformity did not have an impact on these results but there could be other activities where it is important and those should be examined.

Conclusions:

This study examined the relative importance of TF articulation and tray design factors on the initial fixation and micromotion of cementless tibial trays during activities of daily living. Overall, TF conformity greatly influences micromotion and the cause of that seems to be the increased femoral condyle translations increasing the moment arm around the tray. Removal of individual fixation features did not have the impact expected because friction on the plateau appeared to compensate for the missing features. Axial and shear forces through the pegs and stem are controlled by different factors. Axial forces are determined by tray design while shear forces vary with the conformity of the TF geometry. This study exposes many avenues for further research.

CHAPTER 4. CONCLUSIONS

This study contributes to the design of cementless TKR by highlighting the influences of the TF articulation on initial tray stability and examining the contributions of individual fixation features. Previous studies examined micromotion on the exterior rim but only measured compression. This study differentiated between compression of the system and relative motion at the bone-implant interface. Additionally, this study distinguished shear and normal micromotion and highlighted that their effects on bony growth could be different.

This study examined the relative importance of TF articulation and tray design factors on the initial fixation and micromotion of cementless tibial trays during activities of daily living. Overall, TF conformity greatly influences micromotion and the cause of that seems to be the increased femoral condyle translations increasing the moment arm around the tray. Removal of individual fixation features did not have the impact expected because friction on the plateau appeared to compensate for the missing features. Axial and shear forces through the pegs and stem are controlled by different factors. Axial forces are determined by tray design while shear forces vary with the conformity of the TF geometry.

This study included many limitations including the simplified linear-elastic material definitions used in the foam bones, the unrealistic custom inserts created to control conformity, and the treatment of the contact around removed fixation features. A

parametric representation or real tibial inserts could be created to vary TF conformity while still providing realistic geometries away from the insert dwell points. Around fixation features, bone could be removed on the plateau to better simulate degraded bone around a fixation feature and prevent friction forces on that area of the plateau.

This study exposes many avenues for further research using this FE platform, the VIVO simulator, and opportunities for *in vivo* experiments. Future experiments could include natural bone to more accurately examine micromotion around the interface. Additionally, experiments to discover the effects of normal micromotion on bony ingrowth would, along with the results from this study, help inform the designers of TKR what design factors influence boney growth the most.

BIBLIOGRAPHY

Bhimji, Safia, and R. Michael Meneghini. 2012. “Micromotion of Cementless Tibial Baseplates Under Physiological Loading Conditions.” *Journal of Arthroplasty* 27 (4): 648–54. https://doi.org/10.1016/j.arth.2011.06.010.

———. 2014. “Micromotion of Cementless Tibial Baseplates: Keels with Adjuvant Pegs Offer More Stability than Pegs Alone.” *Journal of Arthroplasty* 29 (7): 1503–6. https://doi.org/10.1016/j.arth.2014.02.016.

Chong, Desmond Y R, Ulrich N. Hansen, and Andrew A. Amis. 2010. “Analysis of Bone-Prosthesis Interface Micromotion for Cementless Tibial Prosthesis Fixation and the Influence of Loading Conditions.” *Journal of Biomechanics* 43 (6): 1074–80. https://doi.org/10.1016/j.jbiomech.2009.12.006.

Clary, Chadd W., Clare K. Fitzpatrick, Lorin P. Maletsky, and Paul J. Rullkoetter. 2013. “The Influence of Total Knee Arthroplasty Geometry on Mid-Flexion Stability: An Experimental and Finite Element Study.” *Journal of Biomechanics* 46 (7): 1351–57. https://doi.org/10.1016/j.jbiomech.2013.01.025.

Crook, Paul D., John R. Owen, Shane R. Hess, Samer M. Al-Humadi, Jennifer S. Wayne, and William A. Jiranek. 2017. “Initial Stability of Cemented vs Cementless Tibial Components Under Cyclic Load.” *Journal of Arthroplasty* 32 (8): 2556–62. https://doi.org/10.1016/j.arth.2017.03.039.

Dalury, D. F. 2016. “Cementless Total Knee Arthroplasty.” *Bone and Joint Journal* 98B (7): 867–73. https://doi.org/10.1302/0301-620X.98B7.37367.

Findlay, David M, Katie Welldon, Gerald J Atkins, Donald W Howie, Andrew C.W

Zannettino, and Dennis Bobyn. 2004. “The Proliferation and Phenotypic Expression of Human Osteoblasts on Tantalum Metal.” *Biomaterials* 25 (12): 2215–27. https://doi.org/10.1016/j.biomaterials.2003.09.005.

Fitzpatrick, Clare K., Pleun Hemelaar, and Mark Taylor. 2014. “Computationally Efficient Prediction of Bone-Implant Interface Micromotion of a Cementless Tibial Tray during Gait.” *Journal of Biomechanics* 47 (7): 1718–26. https://doi.org/10.1016/j.jbiomech.2014.02.018.

Fitzpatrick, Clare K., Chase Maag, Chadd W. Clary, Amber Metcalfe, Jason Langhorn, and Paul J. Rullkoetter. 2016. “Validation of a New Computational 6-DOF Knee Simulator during Dynamic Activities.” *Journal of Biomechanics* 49 (14): 3177–84. https://doi.org/10.1016/j.jbiomech.2016.07.040.

Fricka, Kevin B., Supatra Sritulanondha, and Craig J. McAsey. 2015. “To Cement or Not? Two-Year Results of a Prospective, Randomized Study Comparing Cemented Vs. Cementless Total Knee Arthroplasty (TKA).” *Journal of Arthroplasty* 30 (9): 55–58. https://doi.org/10.1016/j.arth.2015.04.049.

Grood, E. S., and W. J. Suntay. 1983. “A Joint Coordinate System for the Clinical Description of Three-Dimensional Motions: Application to the Knee.” *Journal of Biomechanical Engineering* 105 (2): 136. https://doi.org/10.1115/1.3138397.

Harwin, Steven F., Mark A. Kester, Arthur L. Malkani, and Michael T. Manley. 2013. “Excellent Fixation Achieved With Cementless Posteriorly Stabilized Total Knee Arthroplasty.” *Journal of Arthroplasty* 28 (1): 7–13. https://doi.org/10.1016/j.arth.2012.06.006.

Huiskes, Rik, Ronald Rulmerman, G. Harry Van Lenthe, and Jan D. Janssen. 2000. "Effects of Mechanical Forces on Maintenance and Adaptation of Form in Trabecular Bone." *Nature* 405 (6787): 704–6. https://doi.org/10.1038/35015116.

Jasty, Murali, Charles Bragdon, Dennis Burke, Daniel O'Connor, Jay Lowenstein, and William H. Harris. 1997. "In Vivo Skeletal Responses to Porous-Surfaced Implants Subjected to Small Induced Motions." *Journal of Bone and Joint Surgery - Series A* 79 (5): 707–14. https://doi.org/10.2106/00004623-199705000-00010.

Kutzner, I, B Heinlein, F Graichen, A Bender, A Rohlmann, A Halder, A Beier, and G Bergmann. 2010. "Loading of the Knee Joint during Activities of Daily Living Measured in Vivo in Five Subjects." *Journal of Biomechanics* 43: 2164–73. https://doi.org/10.1016/j.jbiomech.2010.03.046.

Navacchia, Alessandro, Chadd W. Clary, Hayden L. Wilson, Yashar A. Behnam, and Paul J. Rullkoetter. 2018. "Validation of Model-Predicted Tibial Tray-Synthetic Bone Relative Motion in Cementless Total Knee Replacement during Activities of Daily Living." *Journal of Biomechanics* 77 (August): 115–23. https://doi.org/10.1016/j.jbiomech.2018.06.024.

Pilliar, R.M., J.M. Lee, and C. Maniatopoulos. 1986. "Observations on the Effect of Movement on Bone Ingrowth into Porous-Surfaced Implants." *Clinical Orthopaedics and Related Research*, no. 208: 108–13.

Proctor, Robert W. 2011. "Playing the Simon Game: Use of the Simon Task for Investigating Human Information Processing." *Acta Psychologica* 136 (2): 182–88. https://doi.org/10.1016/j.actpsy.2010.06.010.

Slover, James, and Joseph D. Zuckerman. 2012. “Increasing Use of Total Knee Replacement and Revision Surgery.” *JAMA* 308 (12): 1266. https://doi.org/10.1001/jama.2012.12644.

Sutton, M. A., X. Ke, S. M. Lessner, M. Goldbach, M. Yost, F. Zhao, and H. W. Schreier. 2008. “Strain Field Measurements on Mouse Carotid Arteries Using Microscopic Three-Dimensional Digital Image Correlation.” *Journal of Biomedical Materials Research - Part A* 84 (1): 178–90. https://doi.org/10.1002/jbm.a.31268.

Valkenburg, Scott M. Van, Frederick W. Werner, Safia Bhimji, Bruce F. White, and Francois B. Asseman. 2016. “Assessment of Physiological Load Testing of Total Knee Implants.” *Journal of Testing and Evaluation* 44 (1): 20140015. https://doi.org/10.1520/JTE20140015.

Wilson, Hayden. 2018. “Cementless Tibial Base Micromotion During Activities of Daily Living.” *Electronic Theses and Dissertations*, January. https://digitalcommons.du.edu/etd/1471.

Yildirim, Gokce, Ananthkrishnan Gopalakrishnan, Robert A Davignon, John W Parker, Harshvardhan Chawla, and Andrew D Pearle. 2016. “Basic Science Comparative Fixation and Subsidence Profiles of Cementless Unicompartmental Knee Arthroplasty Implants.” *The Journal of Arthroplasty* 31: 2019–24. https://doi.org/10.1016/j.arth.2016.02.034.

Zavatsky, A. B. 1997. “A Kinematic-Freedom Analysis of a Flexed-Knee-Stance Testing Rig.” *Journal of Biomechanics* 30 (3): 277–80. https://doi.org/10.1016/S0021-9290(96)00142-X.

APPENDIX 3A: CHANGES IN FIXATION FEATURE FORCES

FIGURES 3A-1-3: CHANGE IN FORCE FROM NOMINAL COMPONENTS FOR SWAPPED COMPONENTS (CYCLE %: GT-16, SD-28, DKB-50)

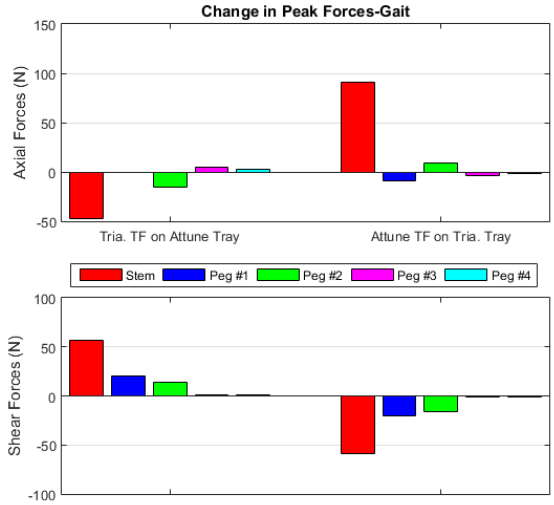

Figure 3A-1

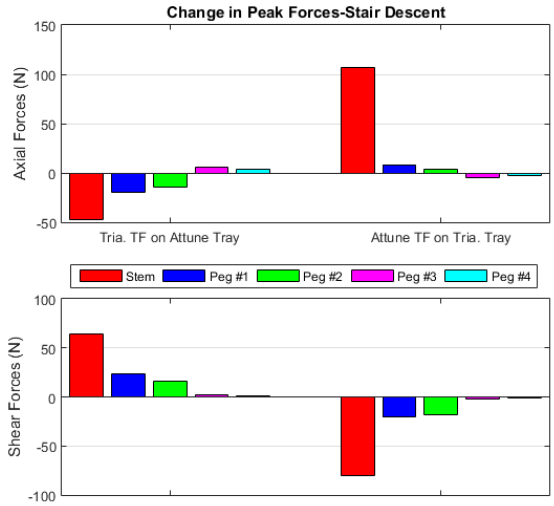

Figure 3A-2

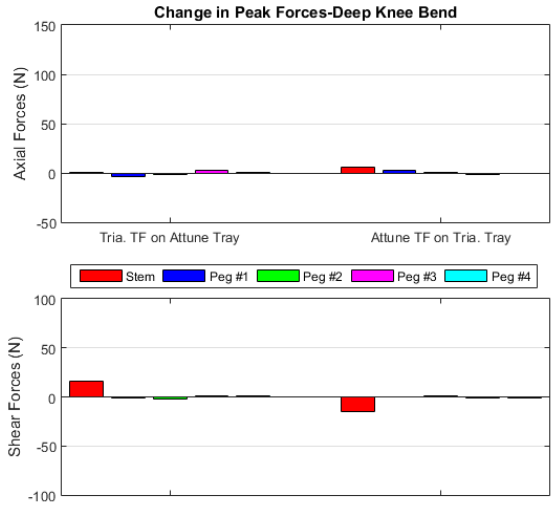

Figure 3A-3
FIGURES 3A.4-9: CHANGE IN FORCE FROM NOMINAL COMPONENTS FOR REMOVED FIXATION FEATURES COMPONENTS (CYCLE %: GT-16, SD-28, DKB-50)

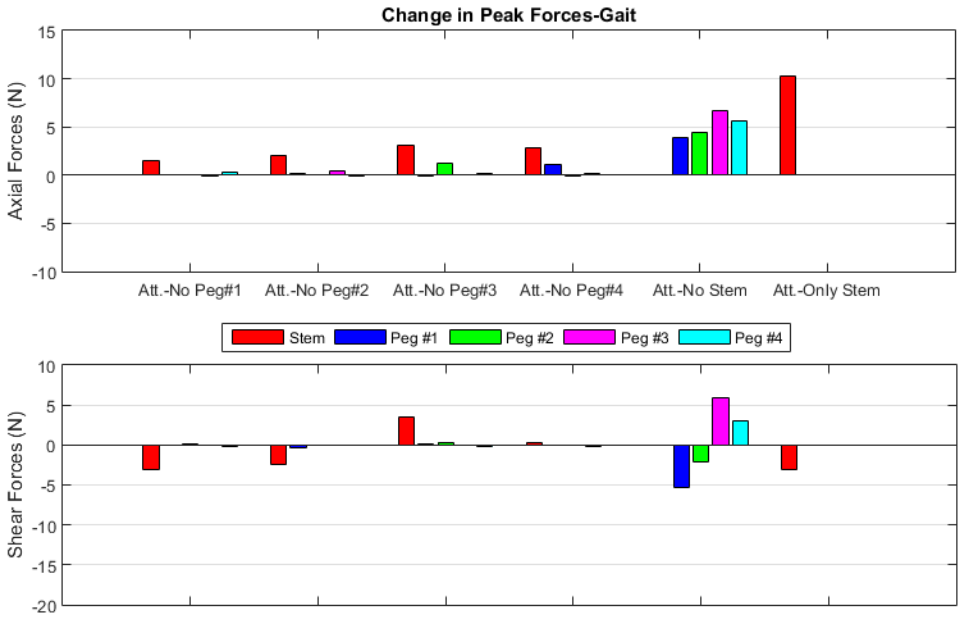

Figure 3A-4

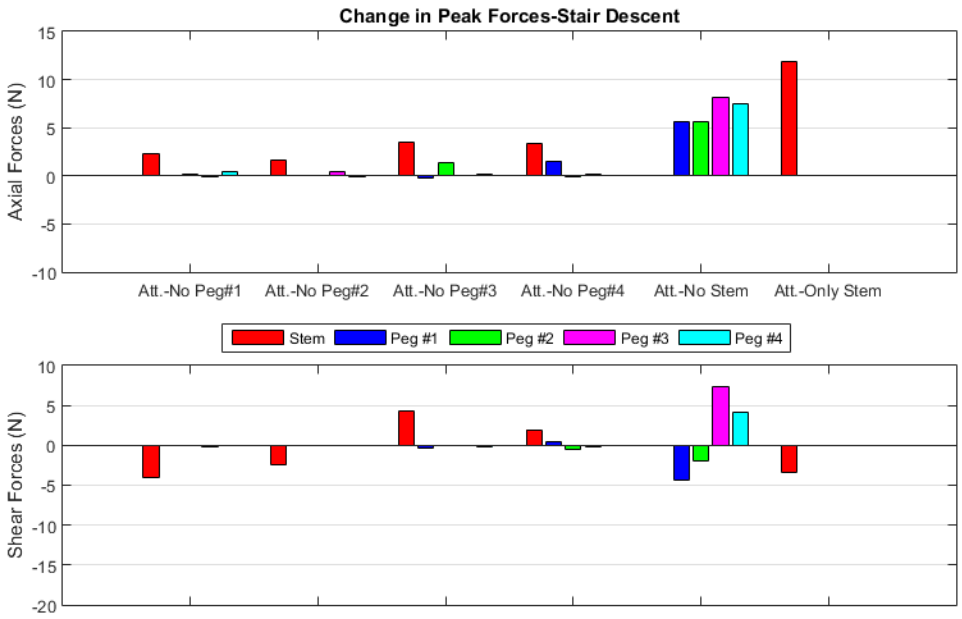

Figure 3A-5

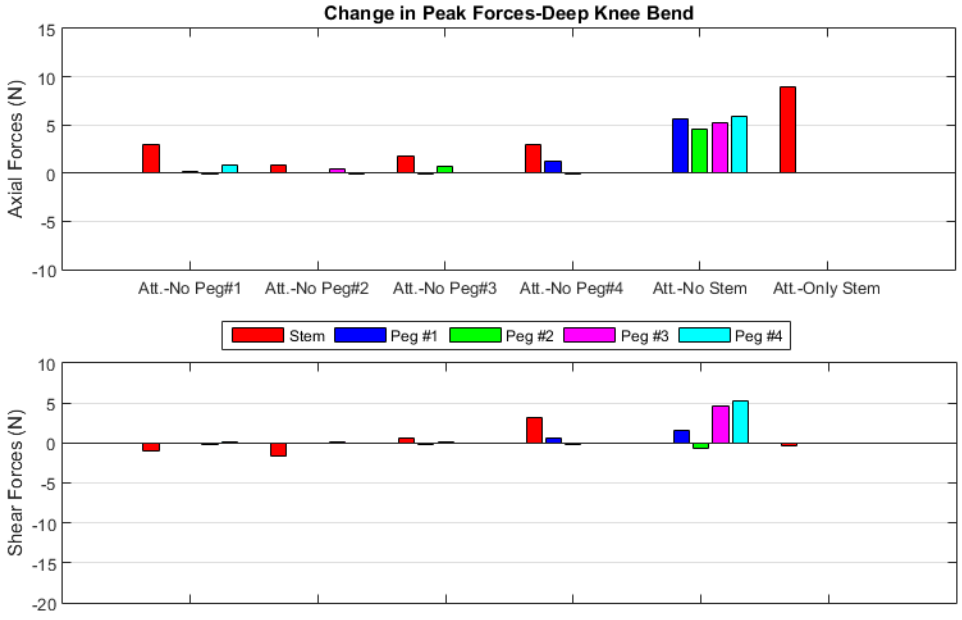

Figure 3A-6

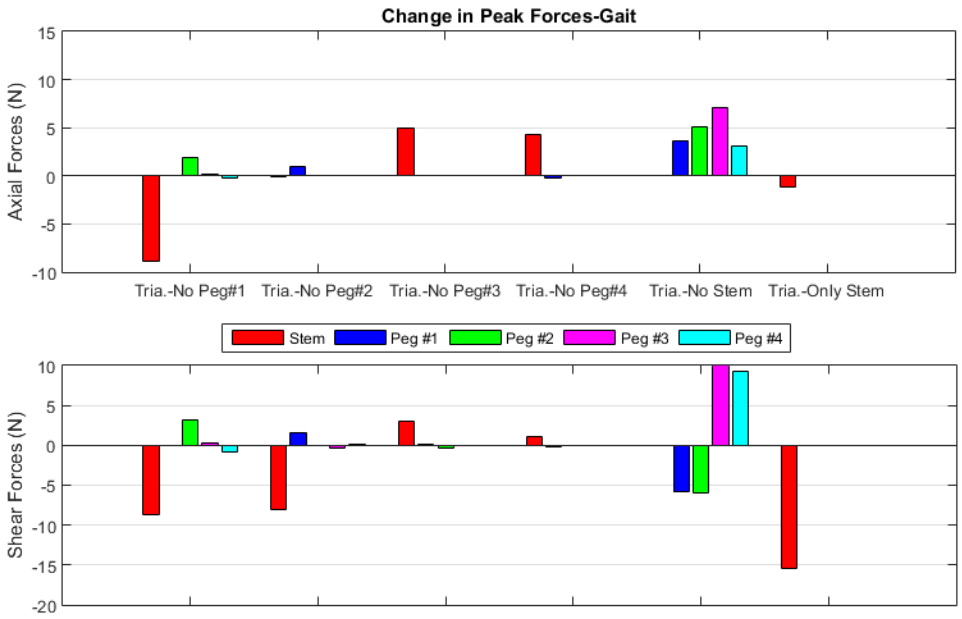

Figure 3A-7

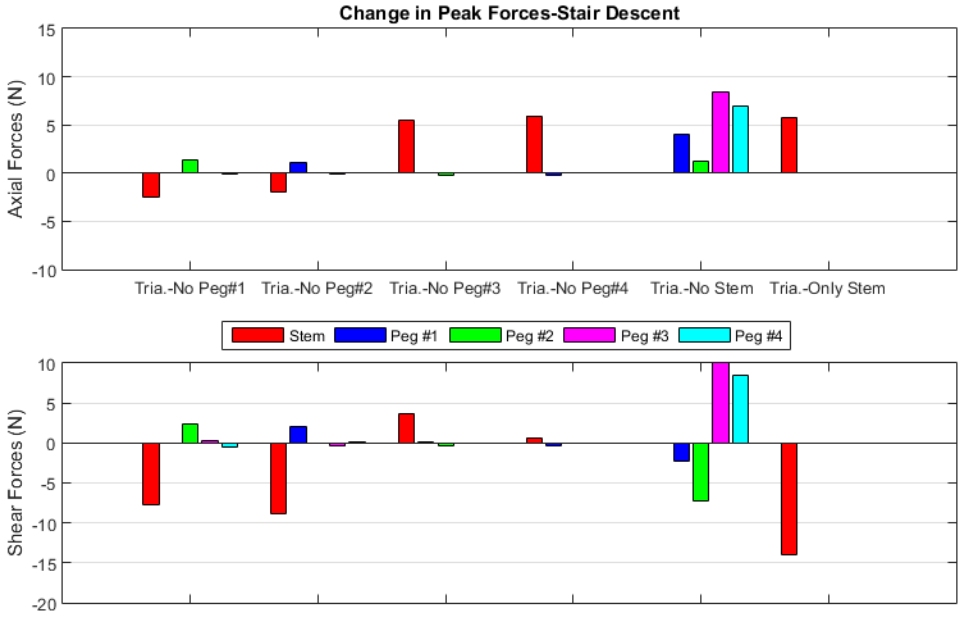

Figure 3A-8

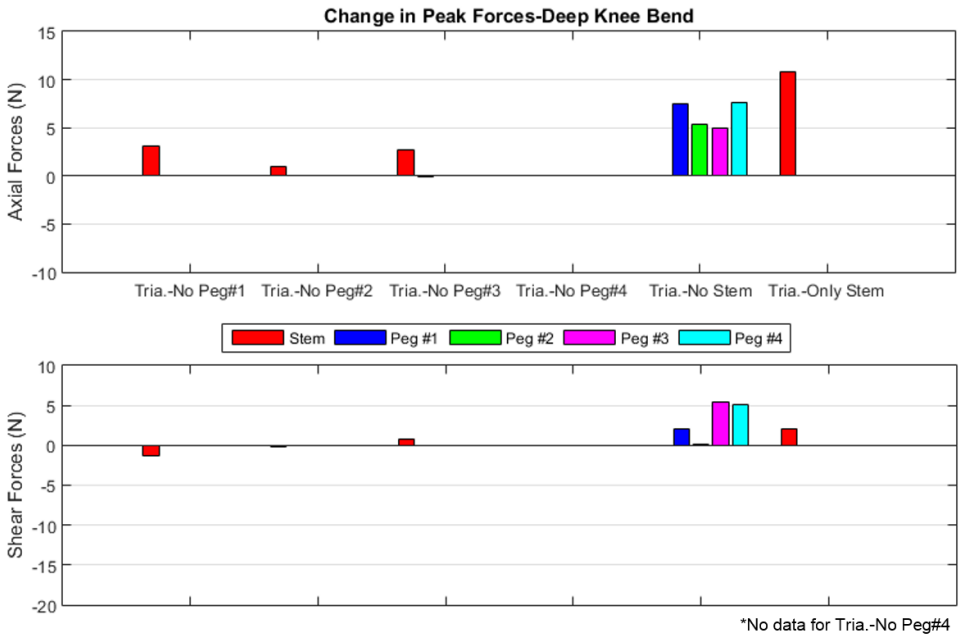

Figure 3A-9

FIGURES 3A-10-15: CHANGE IN FORCE FROM INSERT 2 FOR CUSTOM CONFORMITY INSERTS (CYCLE %: GT-16, SD-28, DKB-50)

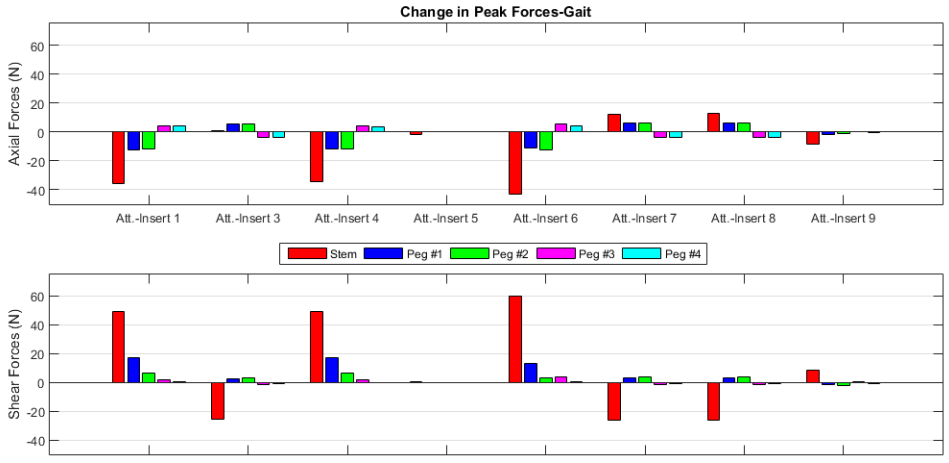

Figure 3A-10

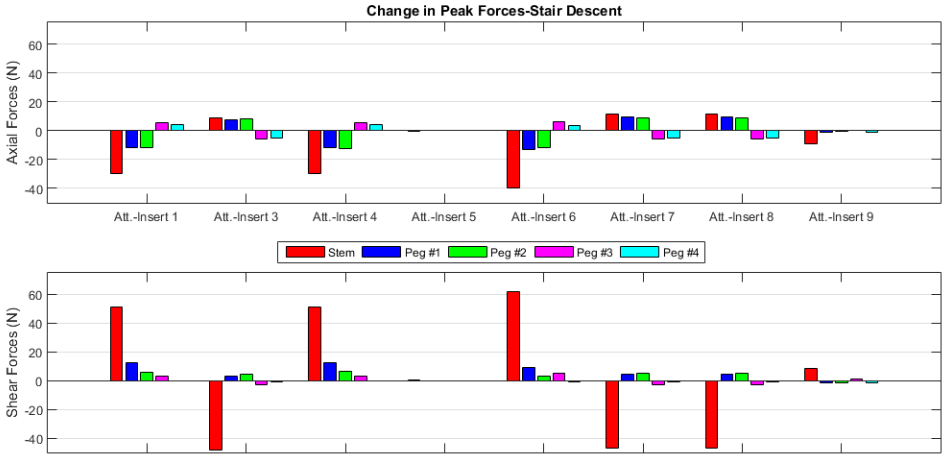

Figure 3A-11

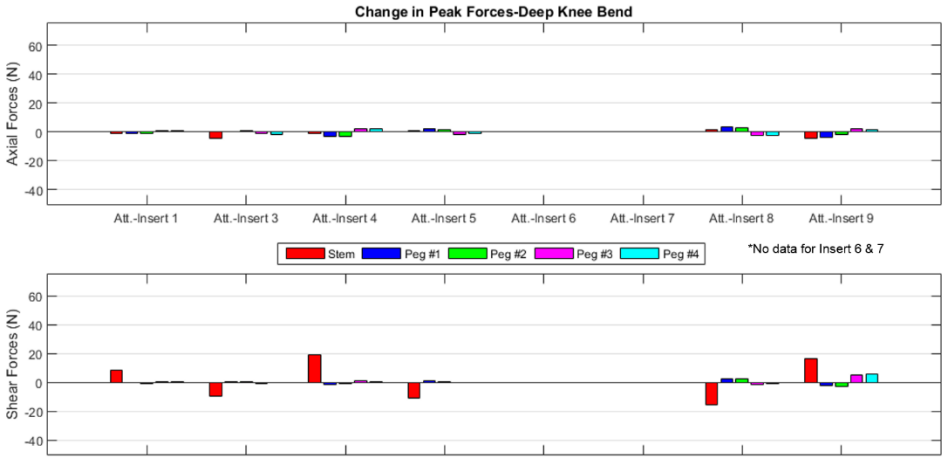

Figure 3A-12

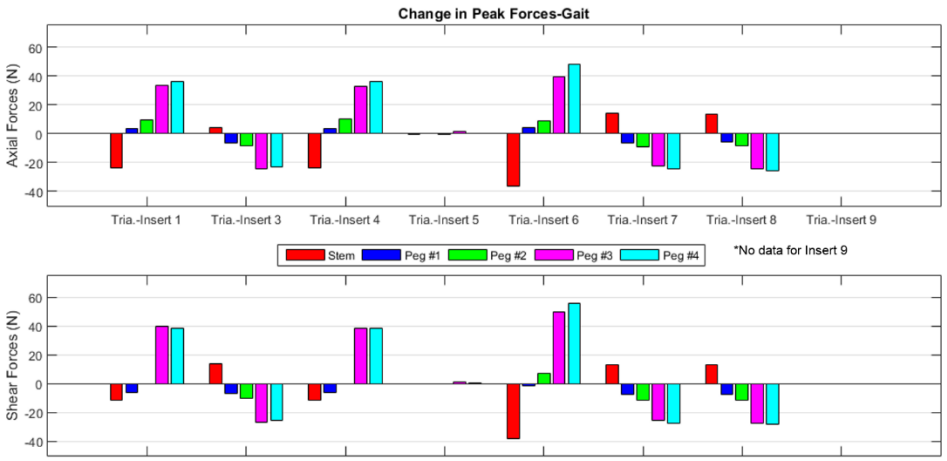

Figure 3A-13

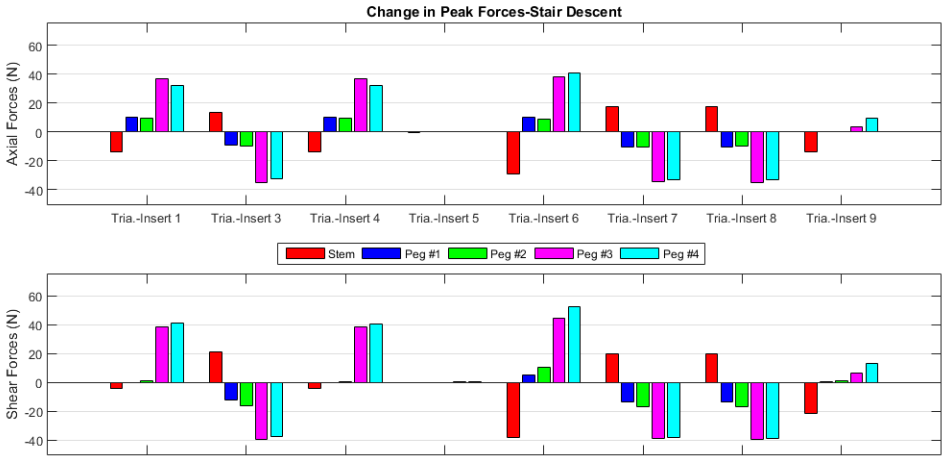

Figure 3A-14

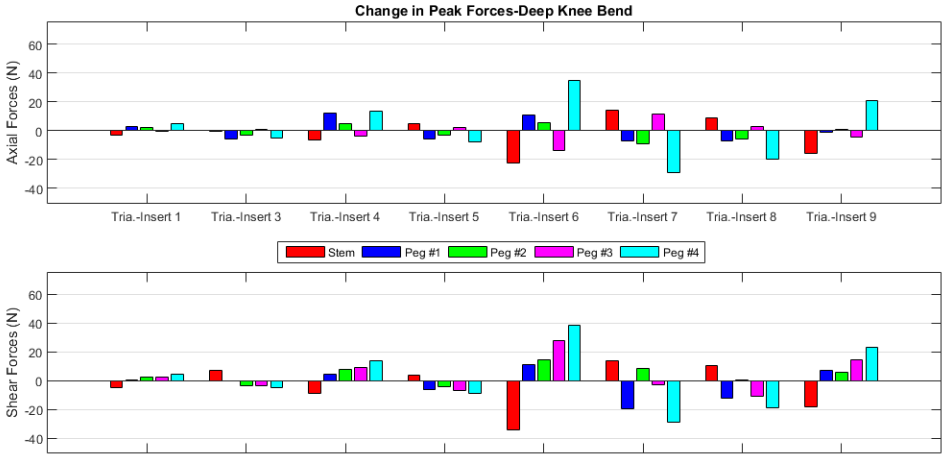

Figure 3A-15

FIGURES 3A-16-21: COMPARISON OF CHANGES IN FIXATION FEATURE FORCES BETWEEN CONFORMRITY AND REMOVING FIXATION FEATURES (CYCLE %: GT-16, SD-28, DKB-50)

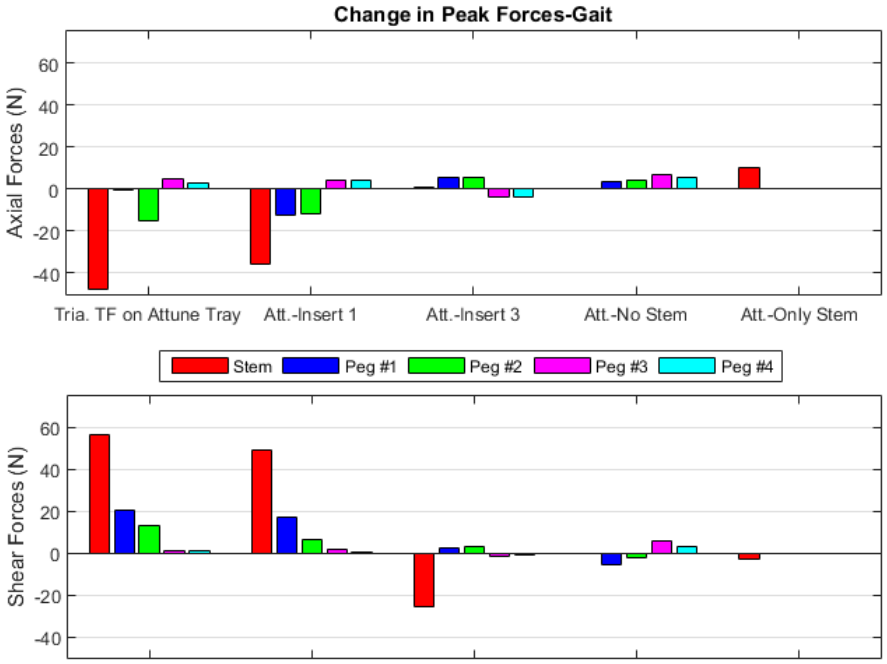

Figure 3A-16

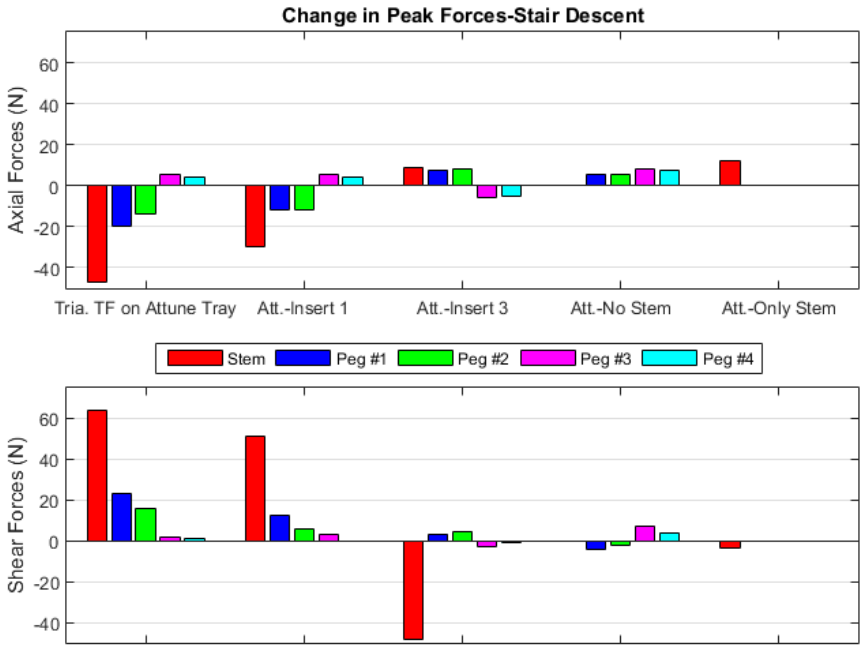

Figure 3A-17

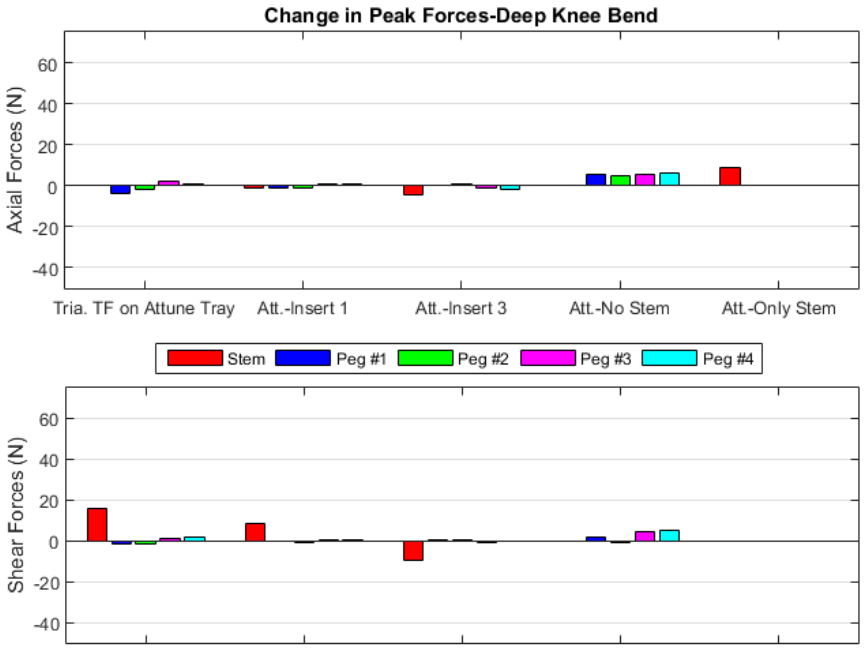

Figure 3A-18

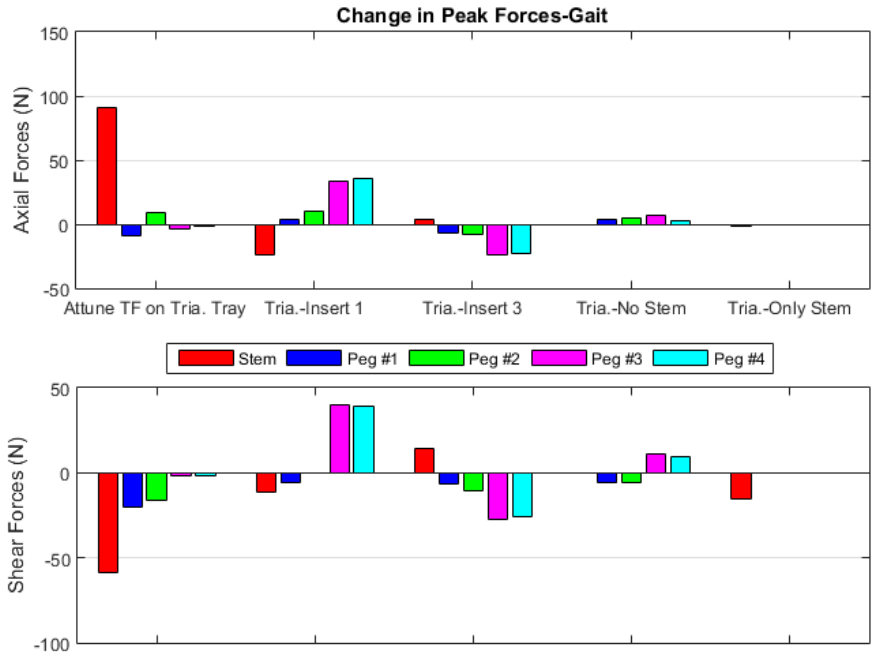

Figure 3A-19

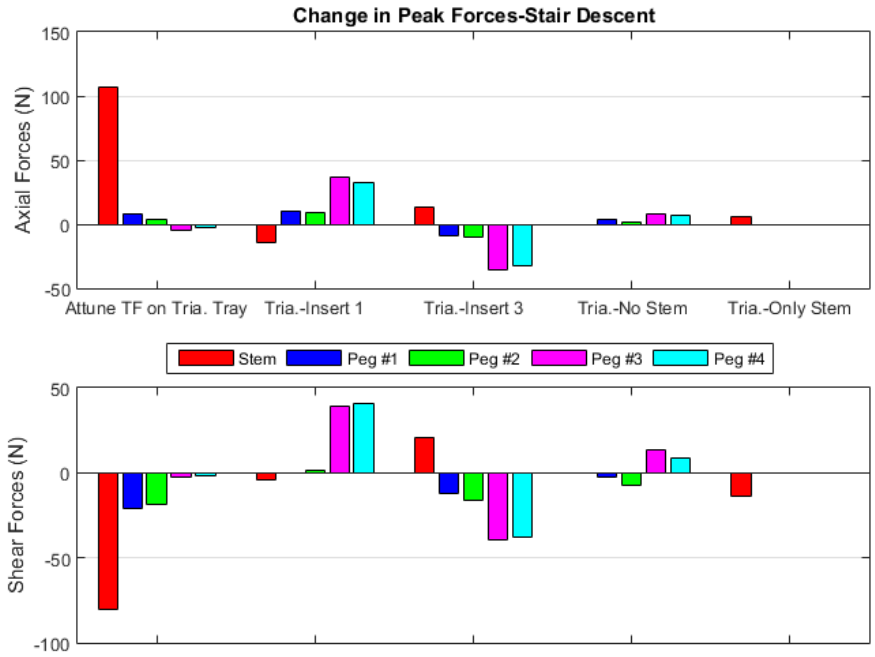

Figure 3A-20

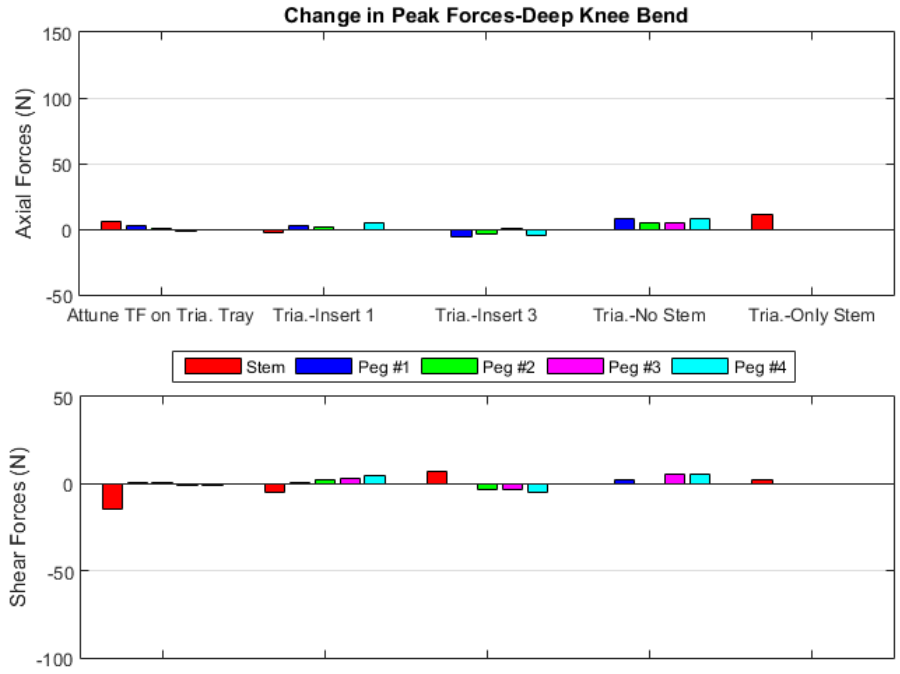
Change in Peak Forces-Deep Knee Bend
Axial Forces (N)
150
100
50
0
-50
Attune TF on Tria. Tray
Tria.-Insert 1
Tria.-Insert 3
Tria.-No Stem
Tria.-Only Stem
Stem
Peg #1
Peg #2
Peg #3
Peg #4
Shear Forces (N)
50
0
-50
-100

Figure 3A-21